The Dissertation Committee for Zhao Chen Certifies that this is the approved version of the following Dissertation:

Human Enzyme-mediated, Systemic Depletion of Methionine for Glioblastoma Treatment

Committee:

John DiGiovanni, Supervisor

George Georgiou

Stefano Tiziani

Karen Vasquez

Lauren Ehrlich

Human Enzyme-mediated, Systemic Depletion of Methionine for Glioblastoma Treatment

by

Zhao Chen

Dissertation

Presented to the Faculty of the Graduate School of

The University of Texas at Austin

in Partial Fulfillment

of the Requirements

for the Degree of

Doctor of Philosophy

The University of Texas at Austin

December 2022

Dedication

To my wife, Qiong

for her companionship and support over the years

Acknowledgements

This dissertation represents the culmination of a long journey that would not have been possible without the assistance of many people. Along the way, I would like to express my sincere gratitude and appreciation to those who have supported me professionally and personally.

First and foremost, I owe my deepest gratitude to my mentor and Ph.D. supervisor Dr. John DiGiovanni, for his unrelenting support in the past six years and continuous optimism concerning this work. Dr. DiGiovanni has guided me through the research process with extreme patience and inspired me to "actively learn" from the frontier of the field. His clear vision, depth of thoughts, clarity of communication and enthusiasm about research not only helped me shape this dissertation, but also motivated me to grow as a full-fledged researcher. Dr. DiGiovanni, thank you! I simply cannot imagine a better mentor.

I would like to convey my sincere gratitude to the members of my dissertation committee for their many constructive suggestions, which have tremendously assisted me in completing this research. I would like to thank Dr. George Georgiou for his support and advice for my research. I would also like to thank Dr. Karen Vasquez for her continued care and support throughout my entire journey since I first moved to the United States. I would like to thank Dr. Lauren Ehrlich for her insightful comments on my project. I owe a tremendous amount of gratitude to Dr. Stefano Tiziani and his team for their collaboration in completing the metabolic analysis required for this work. Without their support, this project cannot be completed.

A special thank you to Dr. George Georgiou and Dr. Everette Stone for engineering this enzyme to make this project possible.

I would like to thank the big family of the DiGiovanni lab. I would like to express my gratitude to Dr. Achinto Saha for his unending patience and guidance during my time in the lab. I would like to thank Carly Wilder, Steve Carbajal, Megha Thakur, Chelsea Friedman, Austin Kindall, Tingzeng Wang, Rachel Clark, Dr. Okkyung Rho, Paige Colbert, as well as former lab members Dr. Lisa Tremmel, Dr. Fernando Eguiarte-Soloman, Dr. Sabin Kshattry, and Dr. Songyoen Ahn, for their friendship, support and encouragement.

I will be eternally grateful for my family's unending love and support. I would like to thank my wife, Qiong, and my parents for their selfless support and companionship. I am grateful to my brother, Yuxin, for helping me maintain my sanity throughout the graduate school journey.

I love y’all.

Abstract

Human Enzyme-mediated, Systemic Depletion of Methionine for Glioblastoma Treatment

Zhao Chen, Ph.D.

The University of Texas at Austin, 2022

Supervisor: John DiGiovanni

Glioblastoma multiforme (GBM) is the most lethal and common type of malignant brain tumor in adults. To date, no curative treatment exists for GBM despite continuous research efforts. Like many other cancers, GBM requires higher levels of methionine for survival compared with normal cells. We aim to exploit GBM methionine dependency as a therapeutic target for this lethal cancer. Our results showed that methionine depletion with an engineered human methionine-γ-lyase (hMGL) reduced GBM cell survival *in vitro*. Metabolic profiling and MSEA revealed that aminoacyl tRNA biosynthesis, glutathione metabolism, and nucleotide metabolism were significantly changed by hMGL treatment. Mechanistic study showed hMGL treatment resulted in notable increases in oxidative stress in GBM cell lines, leading to DNA damage, and caused cell cycle arrest at the S/G2 phase. In line with this thioredoxin reductase inhibitor, auranofin, and the ATR inhibitor, ceralasertib, showed synergistic effects with hMGL in inhibiting GBM cells. Furthermore, hMGL treatment caused a decrease of global DNA methylation and altered histone methylation patterns. This upregulated the expression of tumor-suppressive microRNAs miR-124 and miR-137, which are frequently silenced in gliomagenesis due to aberrant DNA methylation. Accordingly, hMGL inhibited the phosphorylation and activation of

their downstream target, STAT3, a central mediator of GBM growth. Finally, hMGL inhibited the growth of orthotopic human GBM xenografts *in vivo* and prolonged survival time of tumor-bearing animals. Our data provides strong rationale to investigate the efficacy of hMGL in the treatment for GBM.

Table of Contents

List of Tables

List of Figures

Chapter 1: Introduction

1.1 Glioblastoma and current management approaches

Glioblastoma multiforme (GBM) is the most prevalent and deadly malignant primary brain tumor in adults, accounting for 14.2% of all brain and other CNS tumors and 50.1% of all malignant brain tumors.[1,2] The Central Brain Tumor Registry of the United States (CBTRUS), in collaboration with the Centers for Disease Control and Prevention (CDC) and the National Cancer Institute (NCI), estimated that approximately 14,190 cases of GBM will be diagnosed in 2022, and 14,490 cases will be diagnosed for 2023 in the United States.[3] Patients with GBM have a dismal prognosis and quality of life: the median survival time for GBM is less than two years, the lowest among all primary brain and other CNS tumors, and only 6.9% of patients survived five years after diagnosis.[3] In addition, the tumor itself, together with toxicities associated with current treatments, renders more than 50% of survivors dependent on endocrine replacement therapies and more than 75% with permanent neurological deficits.[4]

Despite extensive research efforts, therapeutic advances for GBM over the past two decades have been minimal (**Figure 1.1**).[5] Albeit improvements in surgical and imaging techniques have allowed surgeons to achieve maximal resection with reduced morbidity, a multitude of clinical trials exploring small molecular inhibitors and immunotherapeutic strategies have failed to meet their primary endpoints[6-11]. As a result, gold standard therapy has stayed unchanged since the adoption of temozolomide in 2005[12]; and no novel drug

has been approved by the US Food and Drug Administration (FDA) for the treatment of GBM since the introduction of bevacizumab in 2009[13].

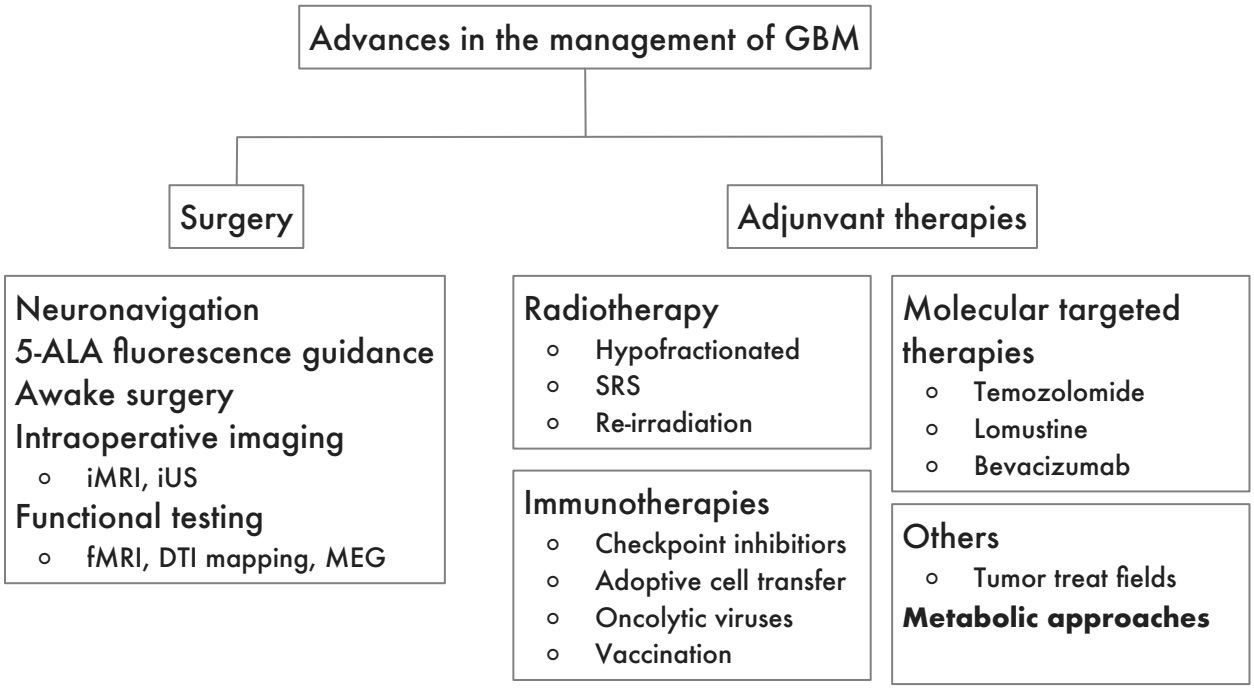

Figure 1.1. Current approaches and advances for the treatment of malignant glioma. 5-ALA, 5-aminoluvulinic acid; iMRI, intraoperative MRI; iUS, intraoperative ultrasound; fMRI, functional MRI; DTI, diffusion tensor imaging; MEG, magnetoencephalography; SRS, stereotactic radiosurgery.

Currently, the standard approach to manage newly diagnosed GBM remains maximal resection followed by concurrent radiotherapy with temozolomide and further adjuvant temozolomide if tolerated.[14,15] There is no standard of care protocol for the treatment of recurrent GBM; potential options include surgery, radiotherapy, and systemic therapy with cytotoxic agents or bevacizumab, etc., depending on the patient's conditions. Unfortunately, the invasive nature of the GBM renders complete surgical resection virtually impossible, and GBM cells are among the most resistant tumors to radiation and cytotoxic chemotherapy[16]. GBM ineluctably recurs, and treatments with meaningful activity in the relapsed settings are largely unavailable.[12,17,18] Novel treatment approaches are desperately needed for this fatal disease.

1.2 METHIONINE DEPLETION AS A STRATEGY FOR GBM TREATMENT

1.2.1 Targeting amino acid metabolism for cancer treatment

Targeting cancer cell metabolism is an emerging alternative method for cancer therapy[19]. To accommodate their increased proliferation, cancer cells rewire metabolic pathways to meet their elevated demands for energy production, biomass accumulation, and reducing agents.[20-22]. Indeed, deregulated uptake of glucose and amino acids is considered one of the hallmarks of cancer metabolism[23,24]; many cancers exhibit autotrophy for specific amino acids and/or become dependent on upregulated de novo synthesis. Such metabolic reprogramming of amino acid metabolism introduces unique metabolic liabilities to cancer cells and presents potential opportunities[19]. Since the first introduction of L-asparaginase for the treatment of pediatric and adult acute lymphocytic

leukemia, different amino acid starvation/depletion strategies have been evaluated for a wide range of malignancies, including dietary restriction, enzymatic depletion of amino acids from serum, blocking of cellular amino acid transporters, and inhibition of key metabolic enzymes. Notably, compared with traditional chemotherapeutics, such strategies have minimal effect on non-cancerous cells because of their lower demand for amino acids and their ability to synthesize the targeted amino acids under conditions of nutrient stress. In addition, these strategies are particularly advantageous in the context of brain tumor treatment since their application is not restricted by the blood-brain barrier[25].

1.2.2 Overview of methionine metabolism

Methionine (Met) is one of the nine essential amino acids in mammals. Met metabolism is a tightly regulated process essential for protein and nucleotide synthesis, intracellular methylation reactions, polyamine synthesis, and maintenance of redox homeostasis[26]. Uniquely, Met can be recycled and salvaged intracellularly in a series of metabolic reactions known as the methionine cycle and the methionine salvage pathway, respectively[27,28]. The methionine cycle starts with the conversion of Met to the universal methyl donor, S-adenosyl-methionine (SAM), catalyzed by methionine adenosyltransferase (MAT) and ATP. Various methyltransferases (MTs) use SAM as a methyl source for DNA, RNA, and protein methylation reactions, thereby regulating epigenetic gene expression and influencing cell signaling activities[29]. SAM is converted to S-adenosyl-homocysteine (SAH) in these methylation reactions, which negatively regulates the SAM-dependent processes. SAH is then converted to homocysteine by

adenosylhomocysteinase (AHCY), which can either fuel the transsulfuration pathway for glutathione synthesis or be remethylated to methionine by methionine synthase (MS), accepting a methyl group from the closely linked folate cycle[30]. Together, the methionine cycle and the folate cycle constitute the two major components of the one-carbon metabolism. In addition, SAM also contributes to polyamine synthesis and nucleotide synthesis, generating 5'-methylthioadenosine (MTA), from which methionine can be recycled through the methionine salvage pathway (**Figure 1.2**).

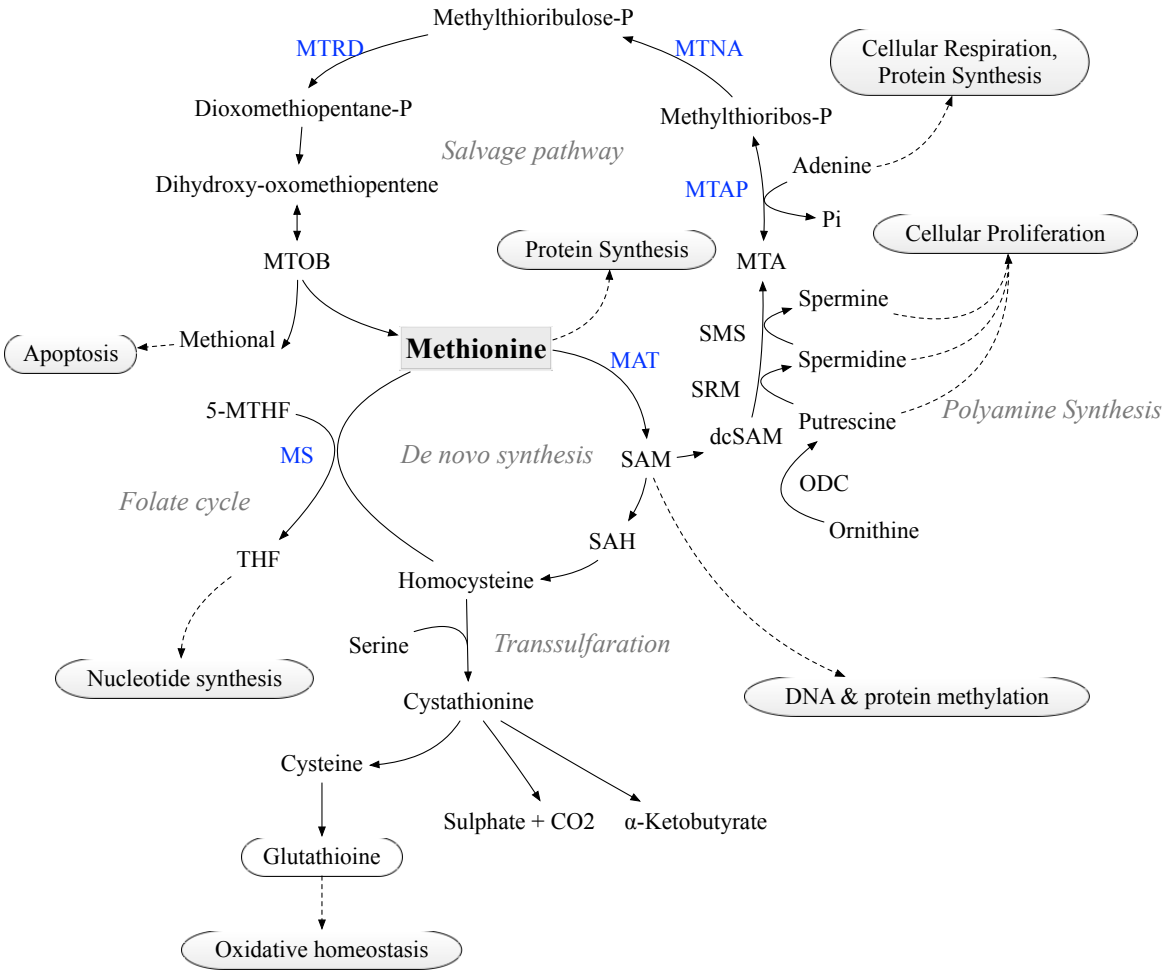

Figure 1.2 Overview of methionine metabolism and related processes. Methionine is catalyzed by methionine adenosyltransferase (MAT) to generate S-adenosylmethionine (SAM), the universal methyl donor. Various methyltransferases (MTs) use SAM as a methyl source to methylate DNA, RNA, and proteins, regulating epigenetic gene expression and influencing protein activities. In this reaction, SAM is converted to S-adenosyl-homocysteine (SAH), which negatively regulates SAM-dependent processes. SAH is then converted by adenosylhomocysteinase (AHCY) to homocysteine, which can either go on to fuel the transsulfuration pathway for glutathione synthesis or be remethylated back to methionine with the help of methionine synthase (MS) and the closely linked folate cycle. Additionally, SAM also contributes to polyamine synthesis and nucleotide synthesis, and methionine can be recycled from the by-product of this reaction, 5'-methylthioadenosine (MTA), through the methionine salvage pathway.

1.2.3 Methionine dependency

Many malignant cell lines and tumors, including glioblastoma, require high levels of Met for survival, growth, and proliferation in a competitive tumor microenvironment. For example, Palanichamy et al demonstrated that methionine metabolism is key to the promotion and maintenance of GBM. In particular, increased demand of methionine is associated with the activation of oncogenes, survival, proliferation, immune evasion and development of resistance for treatment in GBM cells.[31] Indeed, tumors such as GBM are more sensitive to L-Met depletion than their normal counterparts[32,33], and many will fail to survive when the levels of L-methionine fall below a threshold concentration of around ~5 μM from the normal human serum concentration of ~30 μM [34].

This phenomenon, known as "methionine auxotrophy", can be directly observed using positron emission tomography/computed tomography with radio-labeled ^{11}C-

methionine (MET-PET/CT). Increased uptake and accumulation of ^{11}C-MET has been observed in malignancies such as gliomas[35], prostate cancers[36], and certain lymphomas[37], compared with normal tissues and non-neoplastic lesions. In case of gliomas, L-Met traverses the blood-brain barrier and enters tumor cells through L-type amino acid transporters, which are highly expressed in infiltrating glioma cells, but not in normal brain tissue.[38] MET uptake significantly correlates with tumor cell proliferation, vascularization, and consequently tumor grade and patient prognosis[39]. This has led to the widespread adoption of MET-PET/CT in clinical practice for tumor diagnosis and grading [40-42], which has demonstrated high specificity not only in detecting and delineating tumors[43,44], but also in differentiating malignant lesions from benign lesions[45].

1.2.4 Reprograming of methionine metabolic pathways in cancer

In addition to an increased requirement for methionine, many cancer cells also harbor genetic alterations in methionine metabolic pathways, such as increased expression or deletion of Met cycle enzymes. For example, the enzyme responsible for metabolizing Met to SAM, Mat2a, is enriched in tumor-initiating cells[46] and cancer stem cells[47]. Further, N-methyltransferase, an enzyme that utilizes SAM in a reaction to convert nicotinamide to NAD+, has been found to consume methyl groups, diverting SAM from DNA and histone methylation processes (methyl sink) in cancer cells[48]. Additionally, 5-methylthioadenosine phosphorylase (MTAP) acts in the methionine salvage pathway to metabolize methylthioadenosine (MTA) to adenine. MTAP is reported to be deleted in ~15% of human cancers[49]. Changes in enzymes leading to an increase in the polyamine synthesis pathway

have been associated with rapidly proliferating cells and often correlate with poor patient prognosis[50]. One example of an alteration in the polyamine synthesis pathway is the overexpression of ornithine decarboxylase (ODC), which has been observed in many cancer types[51-53]. The enzymatic aberrations in the Met cycle are vulnerabilities that can be exploited for cancer therapy.

Moreover, changes in the Met cycle also contribute to the epigenetic regulation of cancer cells since Met is the immediate precursor for SAM, the universal methyl donor. The methylation of cytosine residues in cytosine-phosphate-guanine (CpG) islands by DNA methyltransferases (DNMTs) has historically been associated with the repression of gene expression[54]. The methylation of some histone sites is associated with gene expression, while the methylation of other sites is associated with gene silencing[55]. Met availability has also been shown to impact translation initiation via met-tRNA levels[56,57] and mRNA cap methylation[58,59] as well as impact RNA regulation by thiolation[60] and N6-methyladenosine (m6A) status[61]. Although complex methylation processes and their relation to cancer progression are not yet fully understood, the related research collectively indicates that Met metabolism plays a major role in the regulation of cancer epigenetics.

1.2.5 Methionine depletion as cancer treatment

The disparity in L-Met requirement between normal and malignant cells provides a clinically meaningful window of opportunity for treating these otherwise intractable cancers with minimal dose-limiting toxicities and adverse effects. Similar to other amino acid depletion treatments, there are two approaches to starve cancer cells of methionine:

dietary restriction and enzymatic depletion. Several proof-of-concept studies have demonstrated the efficacy of methionine depletion in cancer treatment. For example, patients with advanced gastric cancer were given methionine-depleting diets along with chemotherapy for seven days prior to undergoing gastrectomy. While dietary restriction only reduces serum L-Met levels by 40%, this partial L-Met depletion led to a significant reduction in tumor size compared to the control group.[62] Furthermore, in phase I & II clinical trials, dietary L-Met depletion in combination with carmustine for GBM and melanoma was reported to be well tolerated and resulted in improved patient outcomes[63]. Ongoing clinical trials evaluating methionine restriction diet for cancer treatments are summarized in **Table 1.1**.

Table 1.1. Amino acid depletion approaches in clinical trials[64]

Methods	Study	Cancer type/condition	Phases	Reference no.
Methionine-restricted diet	Methionine-restricted diet to potentiate the effects of radiation therapy	Lung cancer, prostate cancer, breast cancer	Not applicable	NCT03574194
Methionine-restricted diet	ONC201 with and without methionine-restricted diet in patients with metastatic triple negative breast cancer	Triple negative breast cancer	Phase 2	NCT03733119
Methionine-restricted diet	A window of opportunity study of methionine deprivation in triple negative breast cancer	Triple negative breast cancer	Phase 2	NCT03186937
Methionine-restricted diet	Dietary methionine restriction plus temozolomide for recurrent GBM	Glioblastoma multiforme	Phase 1	NCT00508456

This table highlights current ongoing clinical trials evaluating amino acid depletion for cancer treatment. The method, brief study design, cancer type, clinical trial phase, and reference number are depicted.

1.2.6 Enzyme-mediated methionine depletion

A more efficient alternative to achieve methionine depletion is using degradative enzymes. Earlier studies demonstrated that enzyme-mediated L-Met depletion using the bacterial methionine-γ-lyase significantly inhibits the growth of GBM, neuroblastoma, colon cancer, prostate cancer, and many other tumors in murine xenograft models[64-67]. This method was initially investigated by isolating L-Methioninase from Clostridium sporogene, which cleaves Met into α-ketobutyrate (α-KG), methanethiol and ammonia[68]. A more stable form of the enzyme, designated rMETase, was isolated from Pseudomonas putida and overexpressed in Escherichia coli to produce large quantities of the enzyme [69]. This variant of the enzyme has been shown to decrease L-Met levels in the serum, resulting in a significant reduction in tumor growth in numerous cancer models. However, the biggest challenge of using pMGL in a clinical setting lies in its heterogeneity: preclinical studies in the macaque model revealed that this bacterial enzyme elicits severe immune responses resulting in anaphylactic shock and death. Additionally, the enzyme rapidly loses activity in serum, necessitating high and frequent dosing for sustained L-Met depletion, conditions that exacerbate the induction of anti-pMGL antibodies[70,71]. Although previous efforts have been made in reducing the immunogenicity of pMGL and increasing its half-life, such as coupling the enzyme with N-hydroxysuccinimidyl ester of methoxypolyethylene glycol propionic acid (M-SPA-PEG 5000) and using sustained-releasing Micropumps[72], none of the results were nearly satisfactory. Another strategy to improve the pharmacokinetics properties of this enzyme involves concealing pMGL within red blood cells. However, erythrocyte encapsulated MGL quickly loses its activity when

its cofactor, vitamin B6, is absent.[73] Thus, despite the remarkable potential of pMGL as an antitumor agent, its high immunogenicity and poor pharmacodynamics render it unsuitable for therapeutic use, and no methionine-depleting enzyme has yet reached clinical trials.

1.2.7 Engineered human methionine-γ-lyase

Mammals do not encode enzymes that degrade L-methionine. To overcome the limitations of pMGL, our collaborating group has created a human enzyme with methionine depleting activities using protein engineering methods.[74,75] Human cystathionine-γ-lyase (hCGL), an enzyme from the transsulfuration pathway, is mutated to create the enzyme. Cystathionine-γ-lyase catalyzes the α, γ-elimination of L-cystathionine to L-cysteine (L-Cys), α-ketobutyrate, and ammonia. With 61% amino acid identity, this is the closest human homolog to pMGL, despite lacking catalytic activity towards L-Met. Using phylogeny-based protein engineering, Lu et al. created a mutagenized variant of hCGL that showed specific degrading activity for L-Met and had 15-fold reduced catalytic activity for its physiological substrate, L-cystathionine. (**Figure 1.3.A**). This engineered enzyme, designated human methionine-γ-lyase (hMGL), carries eight amino acid substitutions to that of hCGL (hCGL - E59I / S63L / L91M / R119A / K268R / T311G / E339V / I353S, **Figure 1.3.B**), and similar to hCGL, hMGL degrades methionine into methanethiol, α-ketobutyrate and ammonium (**Figure 1.3.C**)

In contrast to pMGL, hMGL is extremely stable in serum (with an elimination half-life of 83 ± 2 h) due to its human origin and consequently diminished immunogenicity *in vivo*. A single intraperitoneal injection of 50 mg/kg hMGL into C57/6 mice resulted in a

sustained significant (>75%) decrease of serum L-Met for more than 72 hours without the need of dietary restriction. Importantly, treatment with hMGL inhibited tumor growth significantly in multiple mouse prostate cancer models, while the enzyme was well tolerated by mice as evidenced by the absence of weight loss, liver enzyme abnormalities or other toxicities. Further mechanistic studies demonstrated that prostate cancer cells treated with hMGL exhibited global DNA hypomethylation, DNA damage, cell cycle disturbances, and apoptosis. Given the methionine auxotrophy of GBM, we hypothesize that hMGL-mediated systemic depletion of L-Met will provide significant therapeutic benefits for the treatment of glioblastoma.

A

Variants	L-cystathionine			L-methionine			Ratio L-Met /L-Cyt
hCGL	3.7 ± 0.2	0.4 ± 0.1	9 ± 2	nd	nd	nd	0
hMGL	0.7 ± 0.03	1.2 ± 0.2	0.6 ± 0.1	9.8 ± 0.2	1.8 ± 0.1	5.3 ± 0.5	9

B

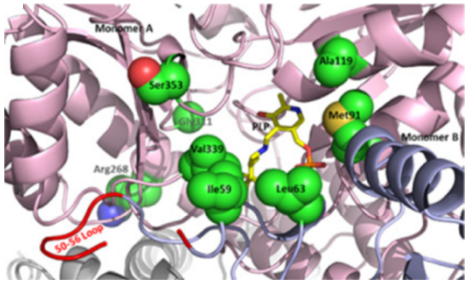

C

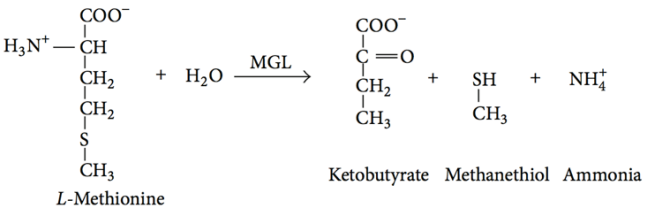

Figure 1.3. Engineered human methionine-γ-lyase A. Michaelis-Menten parameters for engineered hMGL vs. the parent hCGL enzyme. **B**. The location of the mutated residues in hMGL. Residues that were engineered to create hMGL-4.0 that have been shown in space-filling mode. The PLP cofactor is shown in stick with carbon atoms colored yellow. **C**. Enzyme reaction catalyzed by methionine-γ-lyase, which breaks down L-Met to α-ketobutyrate, methanethiol, and NH3. A and B are adapted from *Ref. 75* with permission.

1.3 ENHANCING TREATMENT EFFECTS WITH COMBINATION THERAPIES

Combination therapies usually consist of two or more single therapeutics that act synergistically or additively against cancer cells. The idea of combining single agents was first introduced in 1965, when Frei et al. demonstrated the effectiveness of the combination of methotrexate (purinethol), vincristine (oncovine), 6-mercaptopurine, and prednisone (POMP regimen) in inducing and maintaining remission in children with acute leukemia. The success of the POMP regimen sparked a large amount of interest in the investigation of drug combinations for cancer treatment, which has now become a cornerstone of modern cancer therapy.[76 77]

Drug combinations have the advantage of counteracting compensatory mechanisms of cancer cells by targeting multiple pathways and overcoming unwanted toxicity and other off-target effects associated with high dose of single compounds[78-80]. In the context of methionine dependency, prolonged, extensive methionine restriction is efficient in attaining tumor remission; nevertheless, it faces problems associated with potential toxicity and quality of life issues, and interruption of treatment can result in tumor regrowth.[81]

In addition, the adaptability and plasticity of cancer metabolism poses a significant barrier to targeting tumor methionine auxotrophy or any other metabolic vulnerabilities. For example, under L-Met deprivation, cancer cells can activate autophagy to degrade non-essential cytoplasmic proteins or peptides in order to generate amino acids for their metabolic needs.[82] Certain cancer cells are also able to upregulate transsulfuration or salvage pathways to produce endogenous methionine in the absence of exogenous

sources.[83] In addition, cancer cells can upregulate transporters to compete with immune cells for methionine in the tumor microenvironment, thereby promoting cancer proliferation and sabotaging antitumor immunity.[84] Combination therapies provide crucial opportunities to overcome these barriers by targeting the tumor's compensatory mechanisms.

It is therefore necessary and plausible to investigate hMGL as part of a combination therapy. Indeed, methionine restriction/depletion can act synergistically with other cancer treatments to enhance their efficacy and/or reduce their toxic side effects.

1.3.1 Preclinical research on Methionine Depletion Combinations

One of the first Met depletion combinatorial experiments examined a Met-depleted diet with an antimetabolite analogue, ethionine, which exhibited preclinical efficacy in a prostate cancer xenograft model[85]. However, due to hepatotoxicity the clinical use of ethionine was not continued[86]. Later on, *in vivo* studies have shown that dietary Met depletion enhances the antitumor activity of 5-fluorouracil (5-FU) against Yoshida sarcoma[87] and gastric cancer[62,88]. In addition, preclinical studies have examined the synergistic effects of alkylating agents and enzymatic Met depletion. Results showed that enzymatic L-Met depletion sensitized human brain tumor xenograft models to both N, N'-bis(2-chloroethyl)-N-nitrosourea (BCNU) and temozolomide (TMZ) treatments[89].

Dietary Met depletion has also been evaluated in combination with radiotherapy *in vivo.*[90] In this regard, Miousse et al. demonstrated that the antitumor effects of a Met-

depleted diet combined with radiotherapy were due to effects on one-carbon metabolism, which led to impaired Met biotransformation by downregulating Mat2a. Using an animal model, these researchers also demonstrated that a Met-depleted diet and a diet with low Met levels inhibited melanoma metastasis.[90] A separate study showed that dietary Met restriction (low Met) induces a therapeutic response in radiation-resistant RAS-driven colorectal cancer patient-derived xenografts (PDX) and $KRAS^{G12D}$ + $TP53^{-/-}$driven soft tissue sarcomas.[90] In this study, Gao et al. discovered that the therapeutic mechanism was due to a disruption in one-carbon metabolism affecting nucleotide and redox metabolism, which made cancer cells more sensitive to antimetabolite or radiation intervention.[91]

In preclinical studies, the effects of Met depletion on immune response have also been investigated. Orillion et al. demonstrated that dietary protein restriction (PR) combined with anti-PD-1 treatment significantly inhibited tumor growth both in prostate and renal cancer models.[92] Their group also found that PR combined with PD-1 blockade significantly prolonged survival in an orthotopic renal cancer model.[92] The synergistic effect was attributed to the reprogramming of tumor-associated macrophages from an M2 to a more tumoricidal phenotype with dietary Met restriction.[92] This study provides a rationale for priming the immune system with Met restriction during the initial treatment with immunotherapy.

1.3.2 Dietary Met Restriction in Combination with Anti-cancer Agents in Clinical Trials

As pointed out previously, dietary L-Met restriction in combination with chemotherapeutic agents has been evaluated in numerous preclinical models and several phase I/II clinical trials (**Table 1.1**). In a feasibility study, Durando et al. evaluated a Met-free diet for three two-week cycles with a combined regimen of 5-FU, leucovorin and oxaliplatin (FLOFOX) in patients with metastatic colorectal cancer.[93] During the 30-month follow-up period, three of eleven patients in the study experienced a partial response, and a fourth patient achieved a complete remission.[93] In phase I/II clinical trials, the same group has also evaluated four cycles of a one-day Met-free diet in combination with cystemustine, a chloroethyl nitrosourea agent, in patients with recurrent glioma or metastatic melanoma.[94,95] In these studies, the Met-free diet and cystemustine combination was well tolerated in terms of toxicity and nutrient status. Although the combination did not improve median disease-free survival or median survival in the trial, two patients were able to experience long-duration stabilization.[94,95]

1.4 RESULT SUMMARY

In the current research, we first evaluated the effects of hMGL treatment *in vitro* using multiple GBM cells lines, including cells derived from both adult and pediatric GBMs. Our results show that treatment with hMGL inhibited cell proliferation and induced apoptosis in GBM cells but not in primary glial cell cultures. In order to gain insights into the mechanism-of-action of the antitumor effect of hMGL, metabolic profiling and

pathway enrichment analysis were performed on untreated and hMGL treated GBM cells. Aminoacyl-tRNA biosynthesis, glutathione metabolism, and nucleotide metabolism were among the top enriched metabolic pathways. These were confirmed by results showing that hMGL treatment resulted in notable increases in oxidative stress in GBM cell lines, leading to DNA damage, as evidenced by elevated ROS, decreased GSH, and higher γ-H2AX levels. Cell cycle analysis showed hMGL halted GBM cells at the S/G2 phase.

Given the fact that methionine is the sole precursor to the universal methyl donor, SAM, we also evaluated DNA and histone methylation in GBM cells after hMGL treatment. Our results demonstrated that hMGL treatment caused a decrease of global DNA methylation and altered histone methylation patterns, specifically, decreased trimethylation of histone 3 on lysine 4. The depletion of methionine restored the expression of tumor-suppressive microRNAs miR-124 and miR-137, frequently lost in gliomagenesis due to aberrant DNA methylation. Accordingly, hMGL inhibited the phosphorylation and activation of their downstream target, STAT3, a central mediator of GBM growth.

Finally, since hMGL exhibited significant effects on redox balance and cell cycle, we evaluated the enzyme in combination with compounds that targets antioxidant pathways and cell cycle regulators. Two FDA-approved compounds showed significant synergy with hMGL in inhibiting GBMs *in vitro*: auranofin, a thioredoxin reductase inhibitor, and ceralasertib, an ATR inhibitor.

For *in vivo* validation of the effect of hMGL against GBM, we established an orthotopic GBM xenograft model in mice. Tumor growths were significantly inhibited by

hMGL treatment, and no overt signs of systemic toxicity were observed as shown by the absence of loss of body weight or other neurological side effects.

Taken together, our findings indicate that hMGL exerts antitumor functions, at least in part, by causing oxidative stress, as well as modifying the epigenetic and transcriptional landscape of glioblastoma cells (**Figure 1.4**). The results of this study provide rationale for further mechanistic evaluation and clinical development of hMGL for the treatment of glioblastoma.

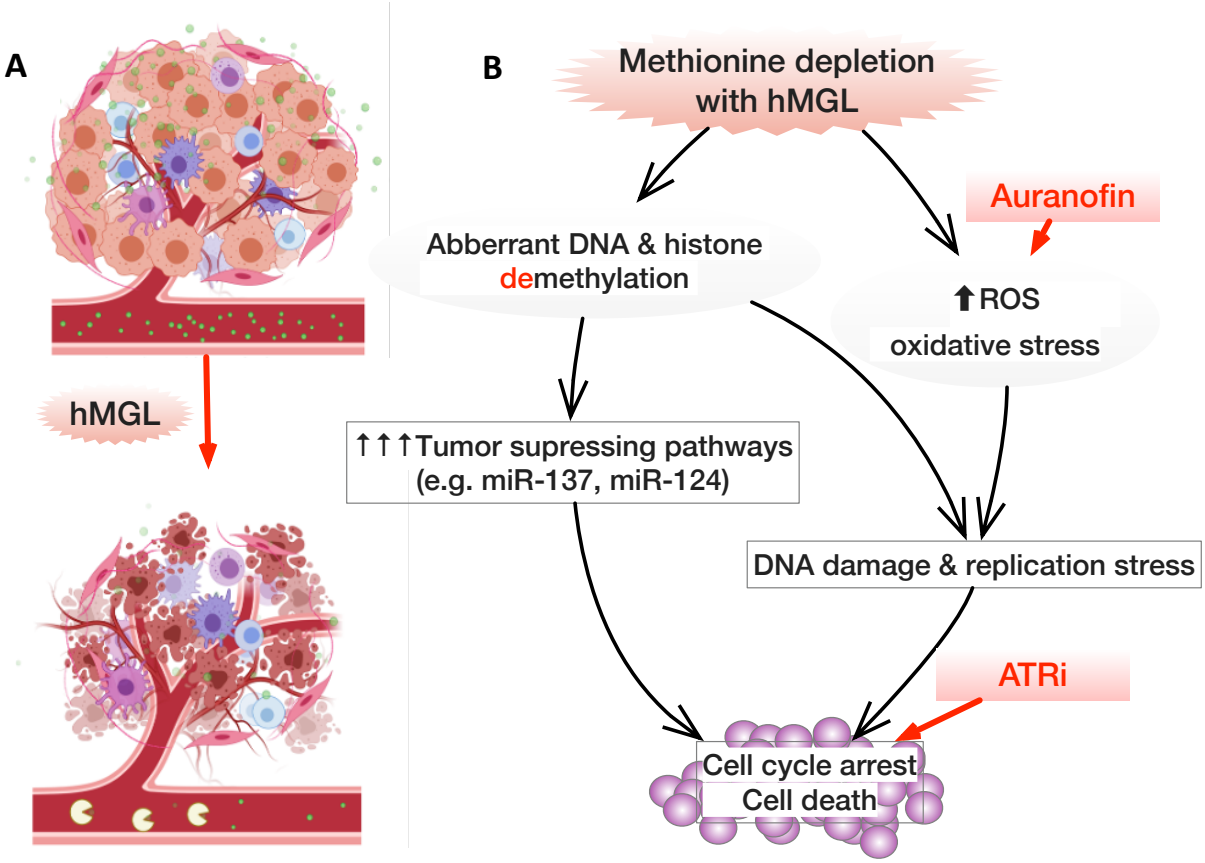

Figure 1.4 Schematic illustration of the tumor inhibitory effect of hMGL. A. Under normal conditions, tumor receive abundant methionine from systemic supplies and from competition with other cells in the tumor microenvironment. Enzymatic depletion of systemic methionine starves the tumor, resulting in cell death. **B.** hMGL exerts its antitumor effects through multiple mechanisms, including affecting epigenetic regulations of tumor suppressive pathways and perturbing oxidative balance.

Chapter 2: Materials and Method

2.1 Chemicals and Reagents

Human methionine-γ-lyase (hMGL) was prepared by the Georgiou lab at UT Austin as previous described[74,96]. AZD6738 (>99%) was purchased from MedChemExpress (Monmouth Junction, NJ). Auranofin (>99%) was purchased from Adipogen (San Diego, CA). N-Acetylcysteine was purchased from Sigma Aldrich (St. Louis, MO).

2.2 Cell lines and culture

U251-luc cell line was kindly provided by Dr. Andrew Brenner from the University of Texas Health Science Center at San Antonio. A172, LN18, T98G, U87G cell lines were purchased from the American Type Culture Collection (ATCC; Manassas, VA). Pediatric high grade glioma cell lines SF188 and SJ-GBM2 was kindly provided by Dr. Jaclyn Hung from the University of Texas Health Science Center at San Antonio. All cell lines were tested for mycoplasma periodically and confirmed to be mycoplasma free using double detection methods: DNA staining with 4,6-diamidino-2-phenylindole (DAPI) and mycoplasma PCR amplification (G-238, Applied Biological Materials Inc).

A172, LN18, T98G, U87G, U251, SF188, and SJ-GBM2 cells were cultured in DMEM/F12 1:1 (Life Technologies) supplemented with 10% fetal bovine serum (Life Technologies) and 1% penicillin/streptomycin (Life Technologies). U251-luc spheroids were derived from the U251-luc cell line. U251-luc cells were cultured in ultralow attachment plates in Neurobasal(-A) medium (ThermoFisher Scientific), supplemented

with B27(-A) (ThermoFisher Scientific), human-bFGF (20 ng/mL) (Shenandoah Biotech), human-EGF (20 ng/mL) (Shenandoah), human PDGF-AA (10 ng/mL) and PDGF-BB (10 ng/mL) (Shenandoah) and heparin (2 ng/mL) (Stem Cell Technologies). All cells were maintained at 37ºC in 95% air and 5% CO2.

2.3 CELL VIABILITY AND COLONY FORMING ASSAYS

Cell survival was measured by Crystal violet assay. Briefly, cells (3,000 to 10,000/mL) in 96-well plates were treated with varying concentrations of hMGL-4.0 or with combinations. At indicated time points, the cells were fixed with 10% formalin and stained with 0.05% Crystal violet. Crystal violet was then aspirated, and cells were washed once with water then the dye was released with 10% acetic acid and absorbance was measured at 595 nm. Relative cell viability was reported by comparing control absorbance to untreated or vehicle treated cells.

For colony formation assay, cells were seeded at low density in 12 well plates and allowed to attach for 24 hours then treatment with various concentrations of hMGL. Plating density is optimized for each cell line and different treating conditions. The resulting colonies were washed twice with PBS, fixed with 4% formaldehyde for 10 min, and stained with 0.1% crystal violet for 30 min.

2.4 *IN VITRO* METABOLOMICS SAMPLE PREPARATION

Cells were seeded at a density of 1.2x106 cells per 150mm dish and allowed to adhere for 24 hours before being treated with hMGL at indicated time points. Cells were

then trypsinized, washed twice with DPBS and pelleted. The cell pellet was immediately flash-frozen in liquid nitrogen and kept at -80°C until analysis. Polar fractions were extracted from cell pellets using a modified Bligh and Dyer technique, and transported to analytical vials for liquid chromatography mass spectrometry (LCMS).[97] The media was diluted with high performance liquid chromatography (HPLC) grade water and transferred to LCMS vials for analysis at a ratio of 1:500. (Polar fractions extraction and LCMS were kindly performed by the Tiziani lab)

2.5 METABOLOMICS SAMPLE ANALYSIS

To track system performance, polar extracts *in vitro* and *in vivo* were spiked with a combination of deuterated internal standards at a ratio of 1:10. The Q Exactive Hybrid Quadrupole Orbitrap mass spectrometer (Thermo Scientific) equipped with electrospray ionization (ESI) in positive/negative ion switch mode was used for polar metabolomics analysis.

The Exactive was used in tandem with the Vanquish Flex UPLC (Fisher Scientific). Mobile phases water and 0.2% formic acid and methanol were used with a Kinetex 2.6 µm C18 100 Å, 150 x 2.1 mm HPLC column (Phenomenex) at a flow rate of 150 µL/min at a ratio of A/B of 98/2 for 4 minutes, 20/80 for 10 minutes, 2/98 for 1 minute, and hold at this ratio for 6 minutes, finally 98/2 for 14 minutes. Redox cofactors were assess using the SeQuant ZIC-HILIC 3.5 µm 100 Å, 150 x 2.1 mm HPLC column. The mobile phases 10mM aqueous ammonium acetate and acetonitrile were maintained at a flow rate of 150 L/min for 12 minutes at a ratio of A/B 90/10. The volume of sample injection was 5 µl.

The following parameters were set on the mass spectrometer: spray voltage, 3.5 kV; capillary temperature, 320°C; sheath gas, 45 (arbitrary units); auxiliary gas, 10 (arbitrary units); m/z range, 70-1000 (HILIC), 50-750 (Kinetex); data acquisition, centroid mode; microscans, 10; AGC target, 1e6; maximum injection time, 200 ms; mass resolution, 70,000 FWHM at m/z 200. The Coenzyme Q analysis was performed as previously described[97].

On imported raw data, SIEVE 2.2.0 SP2 software (Thermo Scientific) was used for peak selecting and spectral alignment. Using an in-house MATLAB script, the integrated peak area, mass to charge ratio, and retention time obtained by SIEVE were exported and matched to a library of standards. Exclusion criteria included a coefficient of variation (CV) greater than 0.25, as determined by the extracted peak areas of repeated sampling of a pooled quality control. Within sample sets, probabilistic quotient normalization (PQN) was utilized for normalizing. (This part of work is performed by the Tiziani lab)

2.6 FLOW CYTOMETRY AND CELL CYCLE ANALYSIS

Before harvesting, cells were treated with varying doses of hMGL for 24 hours. The cells were washed with PBS before being resuspended at a concentration of 2x106 cells per milliliter of PBS. While vortexing, cells were dropwise added to 70% ethanol and kept overnight at -20°C. By resuspending cells in PBS containing Triton X-100 (0.1%, Sigma), RNAse A (100 g/mL, ThermoScientific), and propidium iodide (40 g/mL, Calbiochem) and incubating for 15 minutes at 37o C, cellular DNA was stained. Flow

cytometry was used to acquire the cell cycle phase distribution, which was then analyzed using FlowJo™ v10.8.

2.7 WESTERN BLOTTING

For western blots, cells were washed twice with PBS then lysed in RIPA buffer with 1X protease and phosphatase inhibitor cocktails (Sigma). Protein concentration was quantified using the DC Protein Assay (Bio-Rad) and equal amounts of protein were run in SDS-PAGE gels. Protein was transferred to 0.45 mm nitrocellulose membranes (Bio-Rad). Blots were incubated in 4% bovine serum albumin (BSA) for 1 hour then probed for primary antibodies (listed below) overnight at 4 ºC then secondary antibodies at room temperature for 2 hours. Chemiluminescent detection kits were used to visualize protein on the membranes (SuperSignal West Pico, Thermo Scientific or WesternBright Quantum, Advansta for strong targets; WesternBright Siris, Advansta for weak targets).

Primary antibodies against the following proteins for Western blots were purchased from Cell Signaling Technology (Danvers, MA) p-EIF2-Ser51 (3398), ATF4 (11815), p-UlkSer757 (6888), p-UlkSer555 (5869), Ulk (8054), LC3B (3868), γ-H2AXS139 (9718), H2AX (7631), p-RPASer33 (10148), RPA (35869), p-Chk1Ser345 (2348), Chk1 (2360), Cleaved caspase 3 (9664), cleaved PARP (9548). Antibodies against Ckd4 (sc-56277), Ckd6 (sc-7961), E2F-1 (sc-251were purchased from Santa Cruz Biotechnology; Anti-Histone H3 (tri methyl K4) antibody (ab8580), anti-Histone H3 (tri methyl K27) antibody (ab6002), and anti-Histone H3 (tri methyl K9) antibody (ab8898) are purchased from Abcam (Boston, MA).

2.8 INTRACELLULAR ROS MEASUREMENT

Cells were seeded at desired densities in 96-well opaque plates with clear bottom. Cells were left to adhere to plate overnight and subsequently treated for 24 hours with hMGL alone and in conjunction with NAC. 2',7' Dichlorofluorescein diacetate (DCFDA, Sigma) was added at a concentration of 20 M and incubated for 2 hours at 37ºC to assess cellular ROS. ROS was measured using an excitation wavelength of 485 nM and an emission wavelength of 535 nM, and cell viability was evaluated using the crystal violet method described before. ROS was estimated by standardizing each condition's cell viability and treated culture media without cells.

2.9 TOTAL INTRACELLULAR GLUTATHIONE MEASUREMENT

Total intracellular glutathione (oxidized and reduced) levels were measured using a commercially available Sigma Glutathione Assay Kit (CS0260). Briefly, GBM cells were treated for 24 hours with the given concentrations of hMGL-4.0, washed with PBS, pelleted, deproteinized with 5% 5-Sulfosalicylic Acid Solution, centrifuged to remove precipitated protein, and then tested for glutathione. GSH is quantified using a kinetic assay in which catalytic amounts (nmoles) of GSH induce a continuous reduction of 5,5-dithiobis(2-nitrobenzoic acid) (DTNB) to 5-thio2-nitrobenzoic acid (TNB) and the GSSG produced is recycled by glutathione reductase and NADPH. The present GSSG will react to contribute a positive value to this reaction. The reaction rate is proportional to the glutathione concentration up to 2M, the yellow product TNB measured

spectrophotometrically. The amount of glutathione in a biological sample is determined using a standard curve of reduced glutathione.

2.10 MEASUREMENT OF DNA METHYLATION

The global DNA methylation status was determined colorimetrically using the MethylFlash Global DNA Methylation (5-mC) ELISA Easy Kit after DNA was extracted (P-1030). Briefly, 100 ng of DNA from each sample is bound to strip-wells with a high affinity for DNA. Using capture and detection antibodies, methylated DNA is identified and quantified colorimetrically based on the absorbance obtained by a microplate spectrophotometer. The OD intensity coincides with the percentage of DNA methylation.

2.11 MICRORNA GENE EXPRESSION STUDIES.

TRIzol (Life Technologies) was used to extract total RNA according to the manufacturer's instructions. cDNA was synthesized using a TaqMan microRNA real-time (RT) PCR detection kit (Applied Biosystems). Following the manufacturer's instructions, TaqMan microRNA probe (Life Technologies) was used to detect miR-124, miR-137 from the cDNA for microRNA analysis. Using TaqMan Universal PCR Master mix (Applied Biosystems) and an Applied Biosystems Step One Plus 7500 RT-PCR instrument, microRNAs were quantified in real time. U6 snRNA (TaqMan probe) was used as endogenous internal control.

2.12 MOUSE EXPERIMENTS

To establish orthotopic GBM xenografts, 2 x 105 cells in 5 µl Neurobasal media were injected into the right caudate putamen (CPu, coordination: medium/lateral 2 mm, anterior/posterior 0.5 mm, dorsal/ventral 3.5 mm) of the mice on a stereotaxic apparatus.

Mice were anesthetized using 2-3% isoflurane and secured in a prone position on the stereotaxic apparatus (51730D, Stoelting, co.). A small incision was made to expose the skull and a burr hole was made at the indicated coordinations for the injection. Cells will be injected by a pump controlled micro syringe over 5 min (1µl/min). when injection is completed the burr hole will be sealed with bone wax and incision closed. The mouse will be transferred to a cage (on heat pad), given analgesic and observed until conscious and ambulatory. Mice will be closely monitored for signs of pain, distress, infection or other complications. Additional analgesic will be administered at 24, and if indicated at 48 hr. Mice were monitored for the duration of the experiment and humanely sacrificed when they showed neurological (hemiparesis, paraplegia) or general symptoms (hunched posture, reduced mobility, and/or weight loss > 20%).

Tumor growth was quantitatively measured by bioluminescence imaging starting at day 7. Tumor bearing mice were injected intraperitoneally with luciferin. The IVIS system detects the emitted light with a CCD camera from the luciferase-expressing tumor, yielding a quantitative readout in which light intensity correlates with the number of live cells within a xenograft. The radiance readout, measured in p/sec/cm 2 /sr, is absolute and can therefore be compared across different animals and different experimental time points

as long as all steps of the procedure are conducted the same way. Experiments were terminated when tumor size in the control group reached the maximum limit as specified by the Institutional Animal Care and Use Committee (IACUC) at the University of Texas at Austin. After euthanasia by CO2 blood and tumors were collected for metabolomic analysis.

2.13 GENERAL STATISTICAL ANALYSES

Data are representative of at least three independent experiments unless otherwise stated. Data are expressed as the mean ± standard error of the mean. Sample groups were compared using Student's t test or one-way ANOVA/two-way repeated measures ANOVA followed by Bonferroni's method for multiple comparison test as indicated in the figure legends. Biological replicates were used for every experiment and statistical significance is reported at *$p \leq 0.05$.

Chapter 3: Effect of hMGL treatment on GBM survival, metabolism and signaling pathways

3.1 INTRODUCTION

Our previous studies have shown that hMGL inhibits prostate cancer and melanoma in preclinical models.[75] As a continuation of these previous investigations, we sought to evaluate the efficacy of this human enzyme in GBM models. GBMs exhibit exceptional cellular heterogeneity due to their distinct genetic, epigenetic, and developmental origins.[98] On the basis of transcriptional signatures and genetic abnormalities, the Cancer Genome Atlas Research Network (TCGA) has categorized GBMs into four subgroups: proneural, classical, mesenchymal, and neural.[99] Neftel et al. recently demonstrated, by single-cell RNA sequencing, lineage tracing, and bulk analysis, that GBM cells exist in four biological states that recapitulate diverse neural cell types (neuro-progenitor like, oligodendrocyte-progenitor like, astrocyte-like and mesenchymal-like states).[100] In order to address the issue of heterogeneity, we evaluated the effect of enzymatic L-Met depletion on a panel of GBM cells exhibiting various genetic alterations and phenotypes.

We hypothesized that L-Met depletion could have broad anti-GBM effects by interfering with different aspects of methionine metabolism, and that these anti-GBM effects could synergize with other therapies that have impacts on related pathways. In this chapter, we demonstrate that hMGL selectively inhibits GBM cells by triggering apoptosis while exerting low toxicity on primary glial cells. Aminoacyl-tRNA biosynthesis, glutathione metabolism, and nucleotide metabolism were among the most enriched metabolite sets affected by hMGL-induced methionine depletion, as shown by

metabolomic analysis. Correspondingly, we found that L-Met depletion by hMGL activated the integrated stress response, elevated oxidative stress, and induced cell cycle arrest, all of which contributed to the suppression of GBM survival and proliferation.

3.2 RESULTS

3.2.1 hMGL inhibits GBM cell viability and induces apoptosis *in vitro*

Relative cell survival was measured 48 hours after treatment with different concentrations of hMGL in a panel of GBM cell lines, including adult GBM cell lines A172, LN18, U87MG, T98G, and U251 and the pediatric GBM cell line SF188. Primary mixed glial cultures from adult mouse brain were used as normal control. Both adult and pediatric GBM cell lines displayed a dose-dependent decrease in cell viability in response to hMGL treatment, as measured by the crystal violet assay. Comparatively, primary glial cell cultures were less sensitive to L-Met depletion by hMGL than GBM cell lines (**Figure 3.2.1 A**). To determine if hMGL induces cell apoptosis in GBM cells, the level of cleaved poly (ADP-ribose) polymerase 1 (PARP) was measured at different time points following 250 nM hMGL treatment. Western blot analysis revealed a time-dependent increase in cleaved PARP in tested GBM cell lines, which started at around 6 hours and peaked at 12 hours, indicating an active apoptosis process. (**Figure 3.2.1 B, C**).

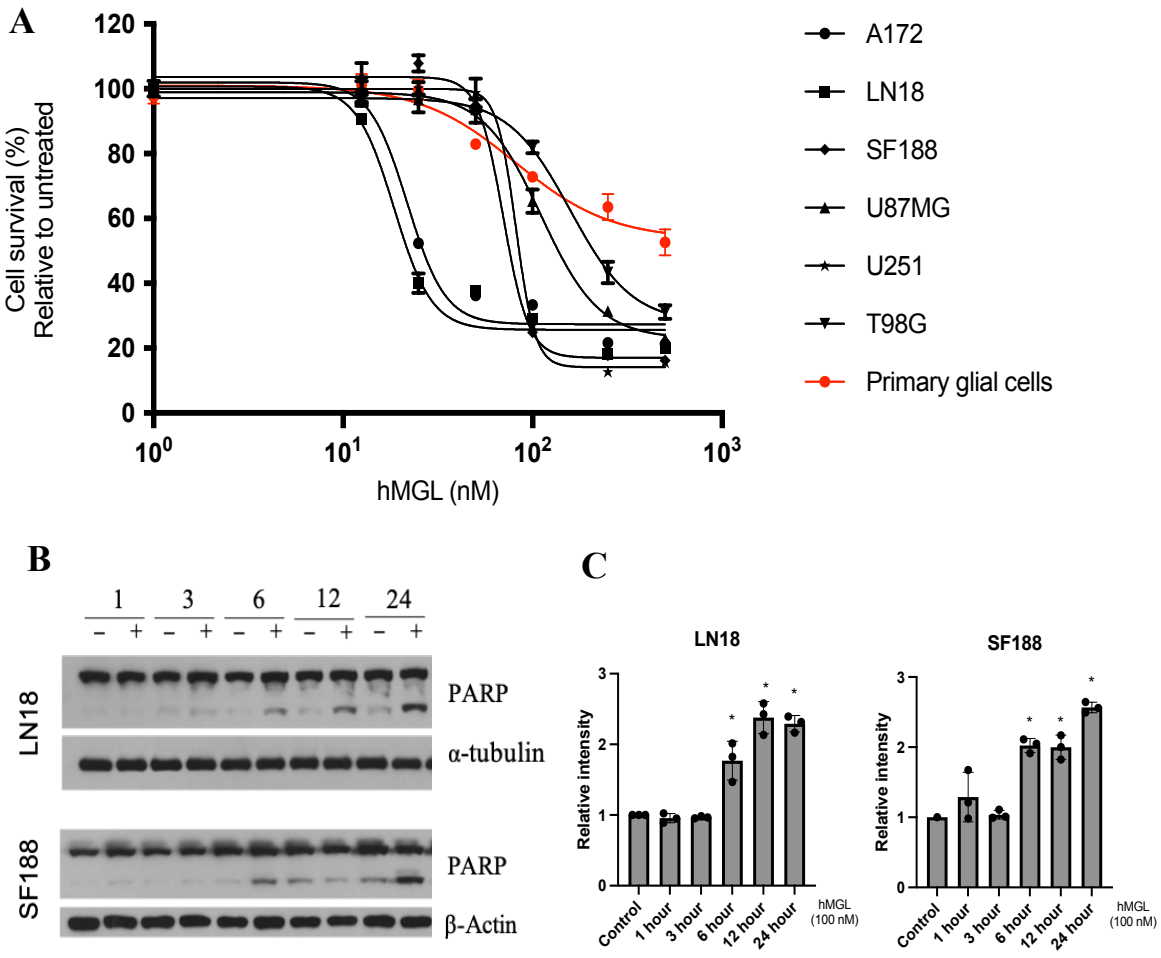

Figure 3.1. **Inhibitory effect of hMGL on GBM cell lines. A.** Relative cell survival after hMGL treatment in adult GBM cell lines A172, LN18, U87MG, T98G, and U251, pediatric GBM cell line SF188, and primary mouse glial cells. Cell viability was measured with crystal violet assay at 48 hours after treatment with hMGL. (Each data point represents nine biologically independent samples from three independent experiments) **B.** Western blots for cleaved PARP in LN18 (adult) and SF188 (pediatric) cells 1, 3, 6, 12, and 24 hours after hMGL treatment and quantification (n = 3 biological replicates per treatment condition). **C.** Quantification of B. Data represents mean ± SEM and Student's t test was used to compare the treated to their corresponding untreated controls at indicated time points. Significance is reported at * $p \leqslant 0.05$)

3.2.2 Intracellular metabolomic changes after hMGL-mediated methionine depletion

To investigate how hMGL-mediated methionine depletion impacts GBM cell metabolism, we collected U251 cell samples 24 hours after treatment with 0 nM, 25 nM, 100 nM, and 500 nM hMGL. Metabolomic profiling of the samples led to the identification of a common group of 168 annotated metabolites in all samples. Obvious differences existed in principle component analysis (PCA) plots among the groups (**Figure 3.2)**. It is worth noting that PC1 separated clearly between control and cells treated with either 100 nM or 500 nM hMGL, and represented 47.6% of the difference, while PC2 also discriminated control and cells treated with 25 nM of hMGL, indicating that hMGL-mediated L-Met depletion affects GBM cells through distinct mechanisms at different enzyme levels. Since the IC50 of hMGL in inhibiting U251 cells is at ~81 nM (**Figure 3.2**), we focused on hMGL 100 nM group for further analysis. Consistent with the PCA analysis, heatmap analysis also clustered obvious distinction between untreated and hMGL-treated groups (**Figure 3.3 A**). Metabolites set enrichment analysis (MSEA) was performed to identify and interpret patterns in the changes of metabolites induced by hMGL treatment, utilizing the web-based tool MetaboAnalyst 5.0 [101,102]. As shown in **Figure 3.3 B**, among the most significantly perturbed metabolic pathways are aminoacyl tRNA biosynthesis, glutathione metabolism, amino sugar and nucleotide sugar metabolism, and purine metabolism. In addition, arginine and proline metabolism, valine,

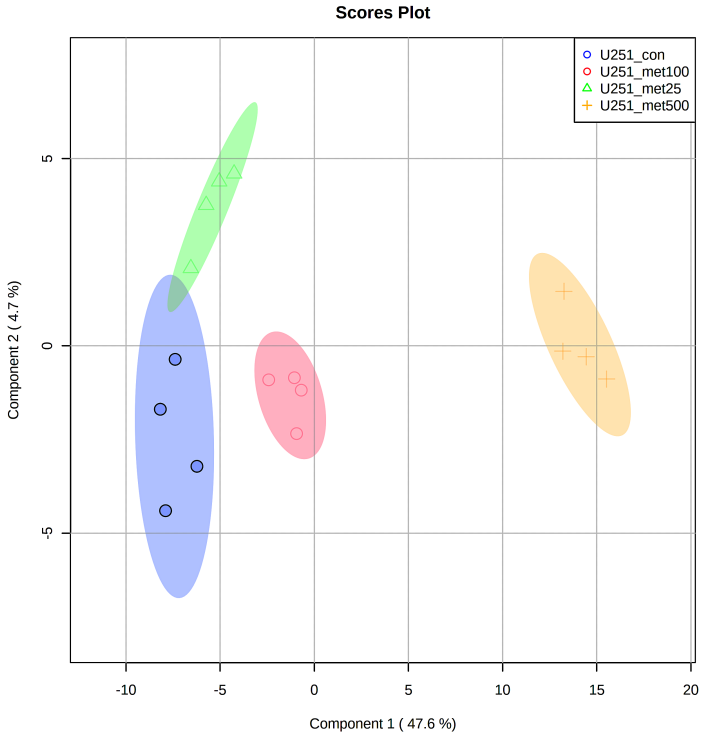

Figure 3.2 PCA plot showing differential metabolites between untreated vs. hMGL treated cells. The control samples (orchid) and cells treated with various dosages of hMGL (25 nM green, 100 nM pink, and 500 nM yellow) are clearly distinguished from one another.

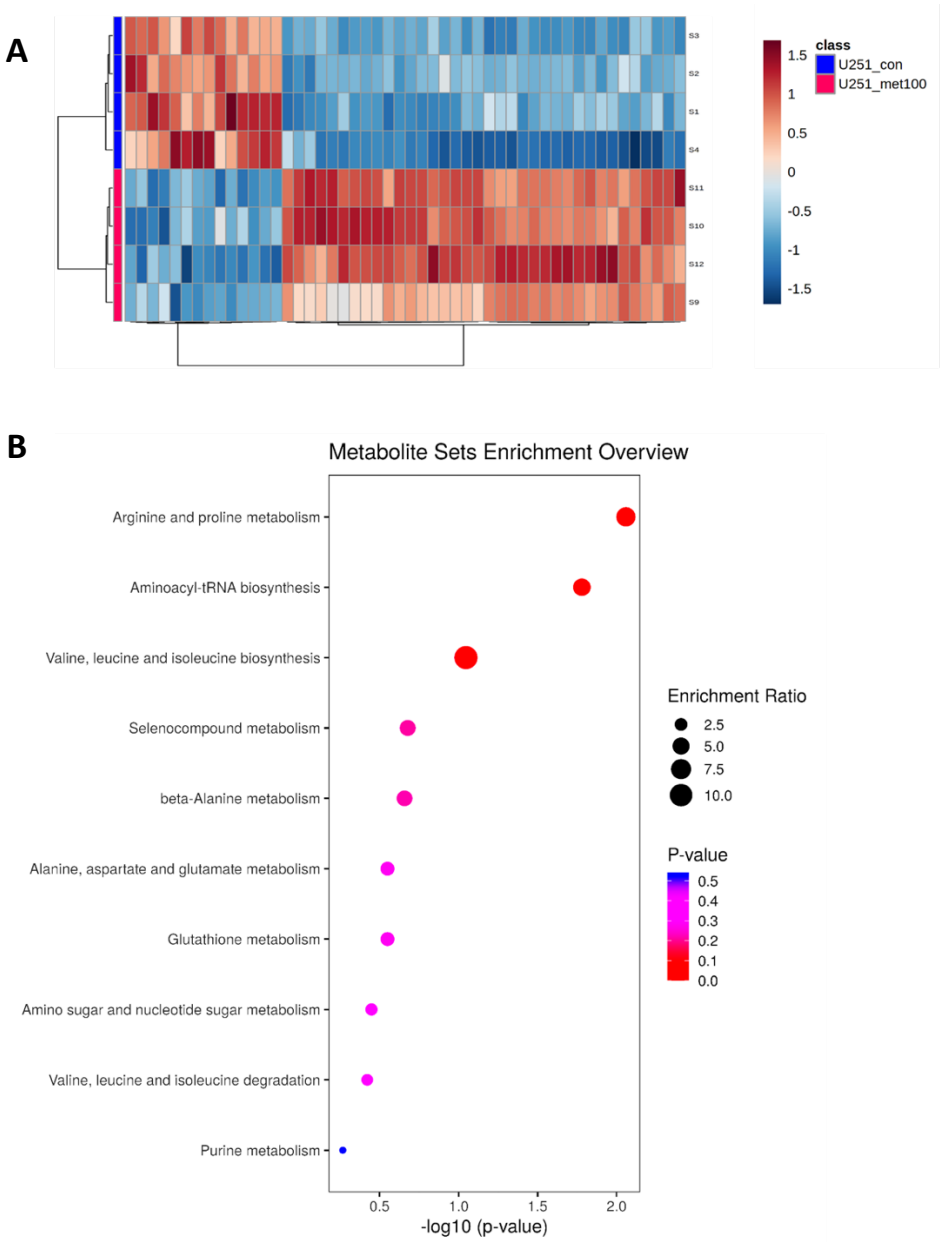

Figure 3.3 Metabolite set enrichment analysis of hMGL induced alterations in GBM cells. Results represent changes in U251 cells after 24 hours of treatment with 100 nM hMGL. **A**. hierarchically clustered heatmap analysis demonstrates obvious distinction between untreated and hMGL-treated groups. The red and blue colors in the heatmap represent higher and lower relative contents than the average value, respectively. **B**. Pathway enrichment using differential metabolites between untreated and 100 nM hMGL-treated GBM cells.

leucine and isoleucine biosynthesis, alanine, aspartate and glutamate metabolism, valine, leucine, and isoleucine degradation were also significantly altered, suggesting that hMGL treatment induced global perturbance in amino acid metabolism in GBM cells.

3.2.3 hMGL treatment stimulated integrated stress response in GBM cells

To conserve cellular energy, protein synthesis is strictly regulated to only occur when amino acids are abundant. Thus, it is essential for the cells to identify deficiencies in essential amino acids for protein synthesis. In mammalian cells, this is accomplished by the conserved general control (GC) system, in which the uncharged transfer RNA induces phosphorylation and inactivation of eukaryotic initiation factor 2 (eIF2) via the GC nonderepressing 2 (GCN2) kinase and/or the protein kinase R-like endoplasmic reticulum kinase (PERK). Phosphorylated eIF2 then suppresses global mRNA translation and induces activated transcription factor (ATF4). ATF4 and its downstream transcriptional targets including Sestrin-2 constitute an adaptive integrated stress response.

Based on our MSEA findings which highlighted significant alterations in aminoacyl tRNA biosynthesis and general amino acid metabolism, we postulated that GBM cells would activate the integrated stress response under hMGL treatment. LN18 cells were treated with 250 nM hMGL for 1, 3, 6, 12 and 24 hours. Western blot analysis revealed that phosphorylation of eIF2α increased three hours after treatment and peaked 12 hours after treatment. Following the phosphorylation of eIF2α, the protein level of ATF starts to increase at six hours after hMGL treatment and maintained the trend until peaking at 24 hours (**Figure 3.4 A**). Moreover, a dose-response experiment with SF188 (pediatric)

and U87MG (adult) cell lines revealed that 24 hours of hMGL treatment led to a dose-dependent increase in eIF2 phosphorylation and that 500 nM of hMGL is sufficient to increase ATF4 protein level in both cell lines (**Figure 3.4 B**).

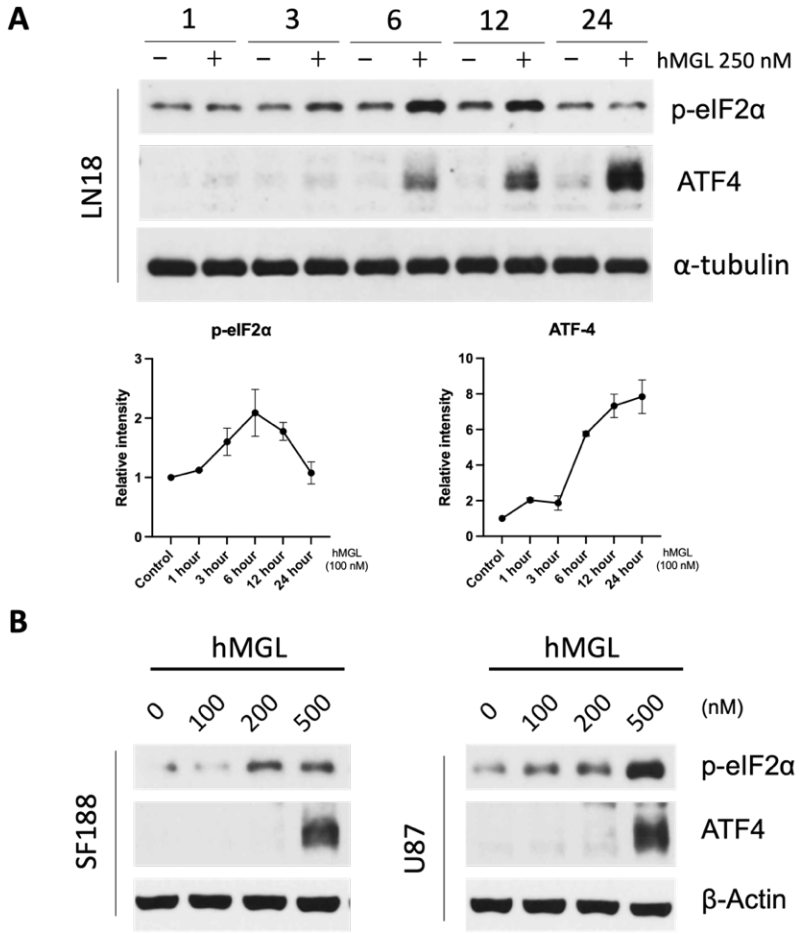

Figure 3.4 hMGL treatment stimulated integrated stress response in GBM cells. A. LN18 cells were treated with 250 nM hMGL for 1, 3, 6, 12 and 24 hours. Western blot revealed that phosphorylation of eIF2α increased three hours after treatment and peaked 12 hours after treatment. Following the phosphorylation of eIF2α, the protein level of ATF starts to increase at six hours after hMGL treatment and maintained the trend until peaking at 24 hours. **B.** In SF188 (pediatric) and U87MG (adult) cell lines, 24 hours of hMGL treatment led to a dose-dependent increase in eIF2 phosphorylation and 500 nM of hMGL is sufficient to elevate ATF4 protein level in both cell lines.

3.2.4 hMGL treatment induces oxidative stress and DNA damage in GBM

The regulation of redox homeostasis is crucial for the maintenance of normal cellular functions and the survival of cells. Cancer cells are characterized by excessively high levels of reactive oxygen species (ROS), also known as oxidative stress, which is caused by their rapid growth and other factors, such as oxygen deprivation and nutrient scarcity. These ROS levels are counteracted by elevated antioxidant defense mechanisms in cancer cells, which include enzymes such as glutathione peroxidase (GPX), thioredoxin reductase (TrxR), and superoxide dismutase (SOD), as well as non-enzymatic antioxidants such as glutathione (GSH), thioredoxin (Trx) and ascorbic acid.

GSH is composed of glutamate, cysteine, and glycine (**Figure 1.2**). As a predominant antioxidant, GSH scavenges ROS and prevents oxidative stress, thereby maintaining redox homeostasis in cells. In addition, GSH is essential for the detoxification of electrophilic xenobiotics such as toxins and drugs. In particular, several types of tumors have been discovered to be resistant to cisplatin due to GSH-mediated detoxification. Loss of GSH will disrupt redox homeostasis and lead to accumulation of reactive oxygen species (ROS), ultimately resulting in dysfunction and death of the cell. As for cancer cells, a high level of oxidative stress makes them more susceptible to GSH deficiency, a fatal flaw that can be exploited in cancer therapy.

As discussed in **3.2.2**, MSEA based on differential metabolites of hMGL-treated GBM cells identified glutathione metabolism as one of the significantly enriched metabolic pathways. Notably, glutamate metabolism, which is interrelated to GSH metabolism by

providing the substrate for GSH biosynthesis was also enriched in the MSEA results (**Figure 1.2**). We hypothesized that hMGL treatment will perturb the oxidative balance and cause cell death by depleting GSH (**Figure 3.5 A**). To investigate the impact of hMGL on redox balance, we measured the levels of GSH and ROS in GBM cells treated with hMGL. Results show that after 24 hours of treatment with 50 nM hMGL, total GSH levels declined significantly. When the concentration of hMGL was increased to 250 nM, GSH dropped to a level that is undetectable (**Figure 3.5 B**). Intracellular ROS of GBM cells treated with hMGL for 24 hours was quantified with 2'-7'-dichlorodihydrofluorescein diacetate (DCFDA) assay. DCFDA diffuses into the cell and get deacetylated by cellular esterase to a non-fluorescent compound, which is then oxidized by ROS into the highly fluorescent 2', 7'-dichlorofluorescein (DCF), which is detected by fluorescence spectroscopy. Results showed that hMGL significantly increased ROS levels across all cell lines tested in a dose-dependent manner (**Figure 3.5 C**). To determine if this perturbance of oxidative balance contributed to reduced survival of GBM cells, we performed rescue experiments with the hMGL treated GBM cells using N-acetyl cysteine (NAC), one of the most widely used antioxidants both in research and in the context of clinical studies. NAC enters the cells and get catabolized to produce hydropersulfides, which acts as direct oxidant scavengers[103]. Notably, the addition of NAC partially rescued all three cell lines from hMGL treatment (**Figure 3.5 D**). Taken together, these results suggest that the disturbance of redox balance in GBM cells, featured by decrease in GSH and increase in ROS contributes to the mechanism of action of hMGL treatment GBM survival.

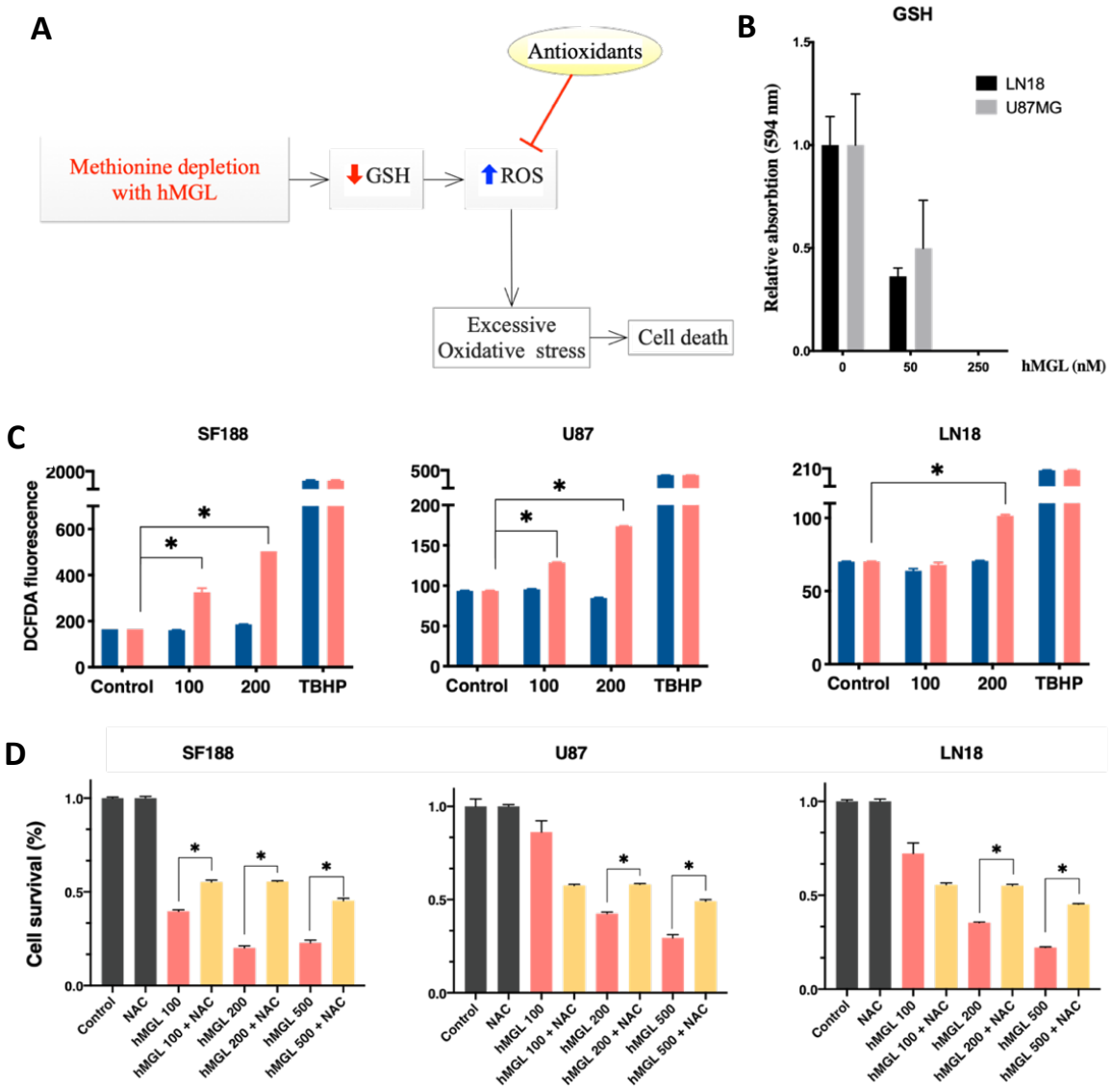

Figure 3.5 The effect of hMGL on oxidative stress hMGL treatment significantly reduces GSH levels and increases ROS levels. **A**. Diagram demonstrating how hMGL treatment affects GSH formation and ROS levels. **B.** Total (oxidized and reduced) glutathione was measured 24 hours after hMGL treatment in LN18 and U87 cells (n=3 biological replicates per treatment condition). **C.** ROS levels were measured 24 hours after hMGL treatment in SF188, U87, and LN18 cells. Tert-Butyl hydroperoxide (TBHP) was used as positive control. For each treatment condition, ROS levels were normalized to media controls without cells and cell viability. (n=2 biological replications per condition). **D.** NAC partially rescued GBM from hMGL treatment. Significance is indicated by * $p < 0.05$.

3.2.5 hMGL treatment induces replication stress and cell cycle arrest in GBM cells

GSH is essential for cellular redox homeostasis and protects DNA from oxidative stress-associated DNA damage. It has been estimated that around 2×10^4 DNA damaging events occur in every cell of the human body every day. A significant portion of the damage is caused by ROS, including direct DNA damage or replication stress-induced DNA damage.[104] Based on our results that hMGL significantly increases oxidative stress in GBM cells, we next measured the effect of hMGL on DNA damage and replication stress. Phosphorylated H2AX (γ-H2AX) can be generated by several kinases, which detect different types of DNA damage throughout the cell cycle, including replication stress that is reflected in activation of the ATR pathway. [105] LN18 and U87 cells were treated with different concentrations of hMGL for 24 or 48 hours, and western blots were used to quantify the level of γ-H2AX after treatment. The results indicate that hMGL treatment increased g-H2AX in both cell lines in a time- and dose-dependent manner (**Figure 3.6 A, B**). The effects of a 24-hour hMGL treatment on the characteristics of the cell cycle in the same cell lines was also evaluated. The proportion of cells in each phase of the cell cycle was determined using PI staining and flow cytometry. In both cell lines treated with hMGL, the percentage of cells in the G1 phase decreased and the percentage of cells in the S phase increased significantly. Histograms demonstrate S-phase aggregation as the concentration of hMGL rises. (**Figure 3.6 C, D**). Taken together, these results demonstrated that hMGL induced an increase in γ-H2AX, which indicates DNA damage or replication stress, and halted the S/G2 phase of the cell cycle.

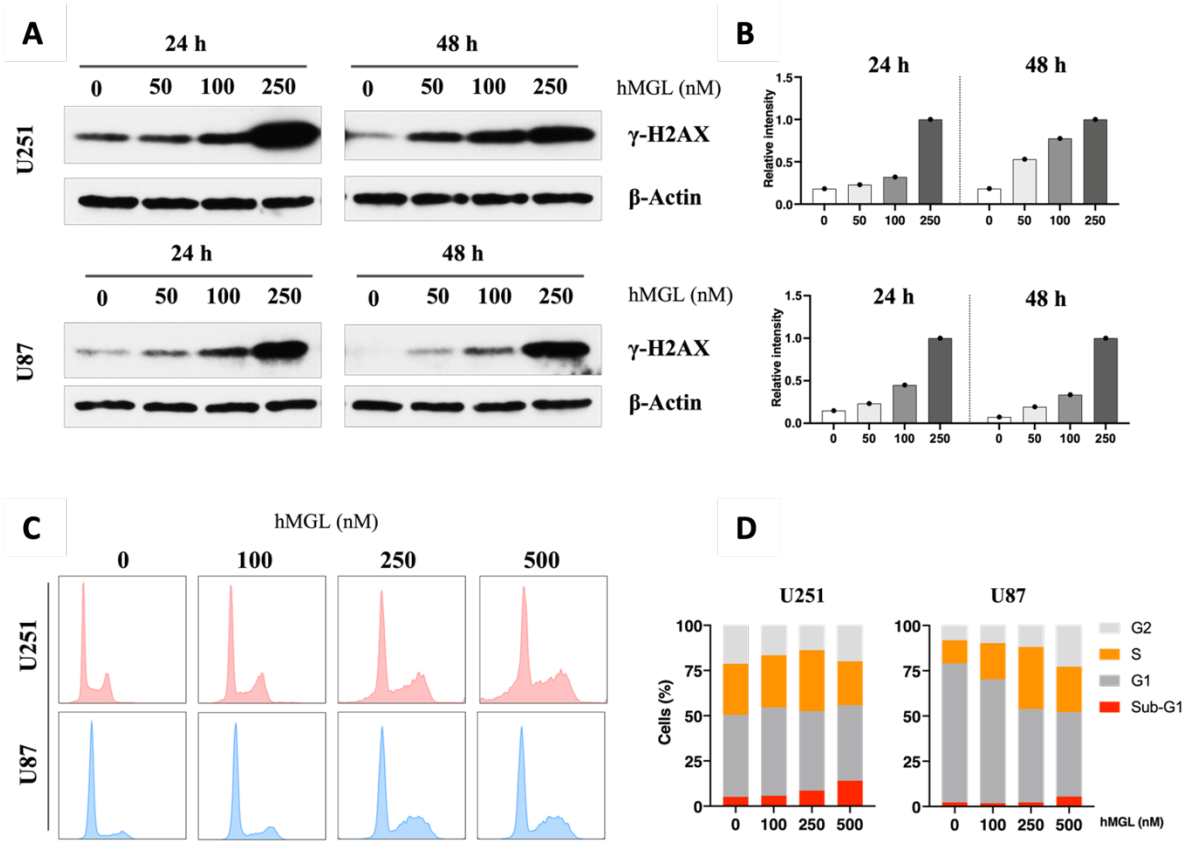

Figure 3.6 hMGL treatment induces replication stress and cell cycle arrest in GBM cells

A and B, Following treatment of LN18 and U87 cells with indicated concentrations of hMGL for 24 or 48 hours, the level of γ-H2AX was quantified using western blots. hMGL increased γ-H2AX in both cell lines in a time- and concentration-dependent manner. **C.** On the same cell lines, the effects of a 24-hour hMGL treatment on the characteristics of the cell cycle were evaluated. Using PI staining and flow cytometry, the proportion of cells in each cell cycle phase was determined. The percentage of cells in the G1 phase decreased and the percentage of cells in the S phase increased significantly in both cell lines treated with hMGL. **D.** Histograms demonstrate S-phase aggregation as the concentration of hMGL rises.

3.3 DISCUSSION

In this chapter, we demonstrated that hMGL treatment specifically inhibited the survival of GBM cells by causing apoptosis while not posing the same level of toxicity on primary glial cell cultures. This is in accordance with a previous report on the methionine dependency of GBM cells,[106] and similar to what has been reported in prostate models.[75] Metabolic profiling provided valuable insights by revealing that aminoacyl tRNA biosynthesis, glutathione metabolism, amino sugar and nucleotide sugar metabolism, and purine metabolism were significantly changed by hMGL treatment.

Following these leads, we discovered that hMGL dramatically decreased GSH levels and induced ROS accumulation in GBM cells. Importantly, we were able to partially rescue the cells from the inhibitory effects of hMGL by using the antioxidant NAC, indicating that ROS plays a crucial role in the mechanism of action of hMGL. ROS has been demonstrated to be a double-edged sword for cancer cells.[107] At low and medium levels, ROS promote the initiation and progression of cancer, whereas as excessive intracellular levels of ROS are detrimental to cell survival, by damaging lipids, proteins and DNA and activating multiple stress signaling pathways. We have observed elevated levels of γ-H2AX, a general marker for DNA damage marker and replication stress. Several mechanisms may contribute to the increase of γ-H2AX, in addition to excessive oxidative stress because of GSH depletion. For example, methionine is the sole precursor for the universal methyl donor, SAM. Methionine depletion will lead to epigenetic changes that alter histones and DNA structure, which will be discussed in Chapter 4.

Another pathway that stood out in the MSEA was the aminoacyl tRNA biosynthesis pathway, which was confirmed by the activation of the eIF2α/ATF4 axis. Briefly, when amino acids are limited, uncharged tRNAs activate GCN2, which in turn phosphorylates eIF2α. EIF2α globally inhibits cap-dependent protein translation except for the translation of a few stress response transcription factors including ATF4. Moreover, the EIF2α/ATF4 axis also reacts to other microenvironmental stresses including oxidative stress, and endoplasmic reticulum (ER) stress. ATF4 promotes adaptation to stresses by transcriptionally regulating amino acid uptake and biosynthesis, autophagy, redox balance, and angiogenesis. Conversely, inhibition of ATF4 impairs amino acid uptake and biosynthesis resulting in increased oxidative stress, cell cycle arrest, induction of apoptosis and delayed tumor growth. This suggest that targeting ATF4 could be a potential therapeutic strategy to use in combination with hMGL.

It should be noted that, given the complexity of L-Met metabolism, hMGL treatment has a much broader effect beyond glutathione depletion and uncharged tRNAs. This is corroborated by our PCA analysis, which showed that the low dose treatment group (hMGL 25 nM) was separated from the higher dose treatment groups (hMGL 100 nM, 500 nM) at different principal components. This highlights the fact that the extent of methionine depletion by hMGL depends on the time of the treatment and concentration of hMGL that was used, and that cells adapt to different levels of methionine via different mechanisms. Further studies are needed to elucidate the contribution of each mechanistic pathway under optimal concentrations and treatment times.

Chapter 4: Effect of hMGL treatment on GMB epigenetics regulation

4.1 INTRODUCTION

Epigenetics broadly refers to heritable alterations in gene expression that are not mediated by changes in the DNA sequence. With breakthroughs in molecular biology over the past decade, it has become apparent that epigenetics is an important contributor to the development and progression of GBM. GBM often exhibits epigenetic abnormalities such as aberrant DNA methylation, incorrect histone modifications, chromosomal remodeling, and altered expression levels of several noncoding RNAs, including microRNAs (miRNA), similar to those of many other malignancies.[108]

4.1.1 DNA methylation

Until recently, the majority of investigations on GBM epigenetic alterations have focused on DNA methylation, one of the earliest identified epigenetic modification pathways.[109] There are four potential DNA methylation sites, including the C-5 position of cytosine, the N-4 position of cytosine, the N-6 position of adenine, and the N-7 position of guanine[110,111]. The majority of DNA methylation in mammalian cells occurs at cytosine of 5′-CpG-3′ in the promoter region to produce 5-methylcytosine (5mC), a methylation reaction catalyzed by DNA methyltransferases (DNMT) using S-adenosyl-methionine (SAM) as methyl donor[112].

In GBM, DNA methylation is characterized by aberrant focal hypermethylation around the promoters of genes and global hypomethylation among nonpromoter elements, which usually results in epigenetic silencing of tumor suppressor genes.[113-116] For example,

around 40% of glioma tissues possess promoter hypermethylation of the DNA repair enzyme O(6)-methylguanine-DNA methyltransferase (MGMT).[117] MGMT antagonizes the genotoxic effects of alkylating agents and promoter methylation is the key mechanism of MGMT gene silencing. The level of MGMT promoter methylation is regarded as the most important measure for determining temozolomide (TMZ) sensitivity in the treatment of glioma. In contrast, downregulation of MGMT might significantly restore the chemosensitivity of TMZ *in vivo* and *in vitro*.[118,119] Other prominent tumor suppressor genes that are usually deactivated by aberrant DNA methylation includes ARF tumor suppressor (p14ARF), Cyclin-dependent kinase inhibitor 2A (CDKN2A/p16INK4α), N-Myc downstream-regulated gene 2 (NDRG2), and Human MutL homolog 1 (hMLH1) and others.[120-123]

In line with this , treatment of GBM xenografts with DNA demethylating agents, such as 5-aza-2′-deoxycytidine (5-aza-dC) and 5-azacytidine (5-aza-CR), yielded encouraging results.[124] Several molecular mechanisms have been proposed to be responsible for the therapeutic effectiveness of DNA demethylation therapies. Recent research has highlighted the reactivation of multiple tumor-suppressor genes simultaneously[125], a process known as epigenetic reprogramming. In addition, sensitization of cancer cells to immunotherapy and chemotherapy has been proposed as a key mechanism of action of DNA demethylating therapies.[126,127]

4.1.2 Histone modification

Histone proteins undergo post-translational modifications (PTMs) such as methylation, acetylation, phosphorylation, and ubiquitylation, SUMOylating, ADP ribosylation, etc. The addition or removal of PTMs from histone is a dynamic and usually reversible process that is mediated by a number of histone-modifying enzymes, including "writers" such as histone acetyltransferases (HATs) and histone methyltransferases (HMTs), and "erasers" such as histone deacetylases (HDACs), histone demethylates (HDMTs/KDMs). Similar to DNA methyltransferases, these chromatin-modifying enzymes are also sensitive to the intracellular availability of intermediary metabolites that serve as their substrates or cofactors, such as SAM or acetyl-coenzyme A (acetyl-CoA). Histone PTMs are recognized by "reader" enzymes and regulate gene expression transcriptionally via altering chromatin states.[128]

Pertaining to the functions of histone PTMs, it is generally accepted that lysine methylation at H3K4, H3K36, and H3K79, as well as arginine methylation, are closely associated with transcriptional activation, while methylated H3K9, H3K27, and H4K20 are associated with transcriptional repression.[129] Nevertheless, the functions of histone PTMs are typically more obscure and complex than they appear on the surface. Occasionally, the markers associated with transcriptional activation may also be associated with transcriptional repression, as is the case with H3K4me3 and H3K36me3.[130,131] Thus, it remains difficult to interpret the transcriptional activity of certain gene loci based on their histone methylation patterns.

In addition to their role in transcriptional regulation, histone PTMs also serve important metabolic functions. One good example is the role of histones as a reservoir of methyl groups. As a "methyl sink", histone contributes to the maintenance of nuclear SAM homeostasis and methylation potential. In the presence of a high concentration of SAM in the nucleus, histone increases the rate of methylation in order to absorb excess methyl groups and minimize aberrant methylation. Histone demethylation, on the other hand, releases methyl groups to compensate for low SAM concentrations in order to meet the needs of other essential processes, such as fueling the nuclear synthesis of GSH through the transsulfuration pathway.[132]

4.1.3 microRNA

MicroRNAs (miRNAs) are a family of small noncoding RNAs that regulate a variety of biological processes via sequence-specific base pairing in the 3′-untranslated regions (UTR) of the target messenger RNA (mRNA), resulting in direct mRNA degradation or translational inhibition. miRNAs play important roles in numerous aspects of cancer initiation, progression, and metastasis, and can act as tumor suppressors or oncogenes.[133-135]

Over the past several years, extensive research has been conducted on the role of miRNAs in gliomagenesis. Global gene expression profiling has revealed the prevalence of aberrant dysregulation of miRNA in GBMs. Numerous tumor suppressor miRNAs, including miR-7, miR-124, miR-128, miR-128, miR-137, miR-181a/b, and mir-138 in GBM, are downregulated in GBMs compared with normal brain tissues. Normally, these

miRNAs regulate cell-cycle progression, apoptosis, DNA repair, or angiogenesis, and their down-regulation is linked to tumor growth and metastasis. Moreover, there are also elevated miRNAs in GBMs functioning as oncogenes, such as miR-21.

The underlying mechanisms of aberrant miRNA expression include chromosomal abnormalities, transcriptional control changes, epigenetic alterations, and defects in the miRNA biogenesis. DNA methylation-mediated regulation of microRNAs is the most intensively studied epigenetic mechanism pertinent to our research. Approximately 50% of miRNA genes are linked to CpG islands. Some of these miRNAs are known to undergo cancer-specific methylation. For example, promoter hypermethylation leads to reduce the expression of miR-124 and miR-137 in GBMs, which are associated with cell differentiation and cell cycle progression. In addition, expression of these microRNAs can be restored by the inhibition of DNA methylation with 5-aza-2'-deoxycytidine (5-aza-dC).[136,137]

In this chapter, we demonstrated that hMGL treatment significantly reduced DNA methylation in GBM cells. Concurrently, histone methylation at H3K4me3, which is known to function as a methyl sink, was reduced. This may serve as a compensatory mechanism to replenish SAM levels that are diminished by hMGL treatment. Parallel to this, we demonstrated that two important tumor suppressive miRNAs, miR-124 and miR137, which are typically downregulated in GBM by promoter hypermethylation, are significantly upregulated by hMGL treatment. These results shed light on the potential epigenetic mechanisms involved in hMGL treatment of GBMs.

4.2 RESULTS

4.2.1 hMGL treatment reduces global DNA methylation.

To determine the effect of hMGL on DNA methylation, U251 cells were treated for 24 hours with 125, 250, and 500 nM of hMGL. Global DNA methylation was evaluated colorimetrically using an ELISA-like reaction and reported as a percentage of 5-mC methylated DNA relative to the amount of input DNA. The results showed that total genomic DNA methylation was comparable between untreated cells and cells treated with low dose hMGL (125 nM). However, when the concentration of hMGL was increased to

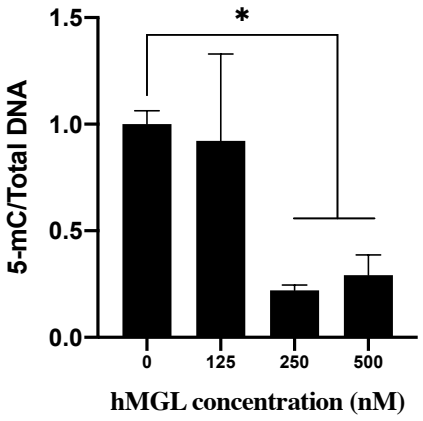

Figure 4.1 hMGL decreases global DNA methylation of GBM cells. Global DNA methylation was measured colorimetrically using an ELISA-like reaction as a percentage of 5-mC methylated DNA to input DNA. Untreated and low-dose hMGL-treated cells had comparable total genomic DNA methylation (125 nM). When hMGL was increased to 250 or 500 nM, global DNA methylation dropped significantly in the treatment group compared to the untreated cells.

250 nM or 500 nM, global DNA methylation levels dropped significantly in the treated cells compared with the untreated cells. This result demonstrated that hMGL treatment induces a dose-dependent reduction in global DNA methylation, suggesting that a compensatory mechanism exists to maintain DNA methylation with low doses of hMGL; however, global DNA methylation decreased when the concentration of hMGL exceeded a certain threshold and methionine levels dropped below a critical threshold.

4.2.2 hMGL treatment alters histone methylation patterns in GBM cells

As described in Section 4.1, Histone methylation is controlled by chromatin-modifying enzymes HMT (writers) and HDMTs/KDMs (erasers). The activity of these enzymes is ultimately regulated by the availability and concentration of their co-factors and substrates, such as SAM, the universal methyl donor.[138] Since methionine is the sole precursor for SAM, we hypothesized that hMGL treatment would lead to changes in histone methylation patterns. To test this hypothesis, U87 cells were treated with 400 nM hMGL for 24 and 48 hours. Histones were acid extracted and histone methylation at H3K4me3, H3K9me3, and H3K27me3 were examined by western blotting. The results showed that hMGL treatment strongly decreased the amount of H3K4me3 in GBM cells. In contrast, H3K9me3 and H3K27me3 were not significantly changed (**Figure 4.2 A, C**). In the pediatric GBM cell line SF188, the hMGL-induced modification of histone methylation followed a similar pattern as that observed with U87 cells (**Figure 4.2 B, D**). In addition, after 24 hours of treatment with 400 nM hMGL, a reduction of H3K4me3 was observed in T98G, however this reduction was not statistically significant. H3K9me3 and

H3K27me3 remained stable in all cell lines after 24 hours of hMGL treatment (**Figure 4.2 B, D**).

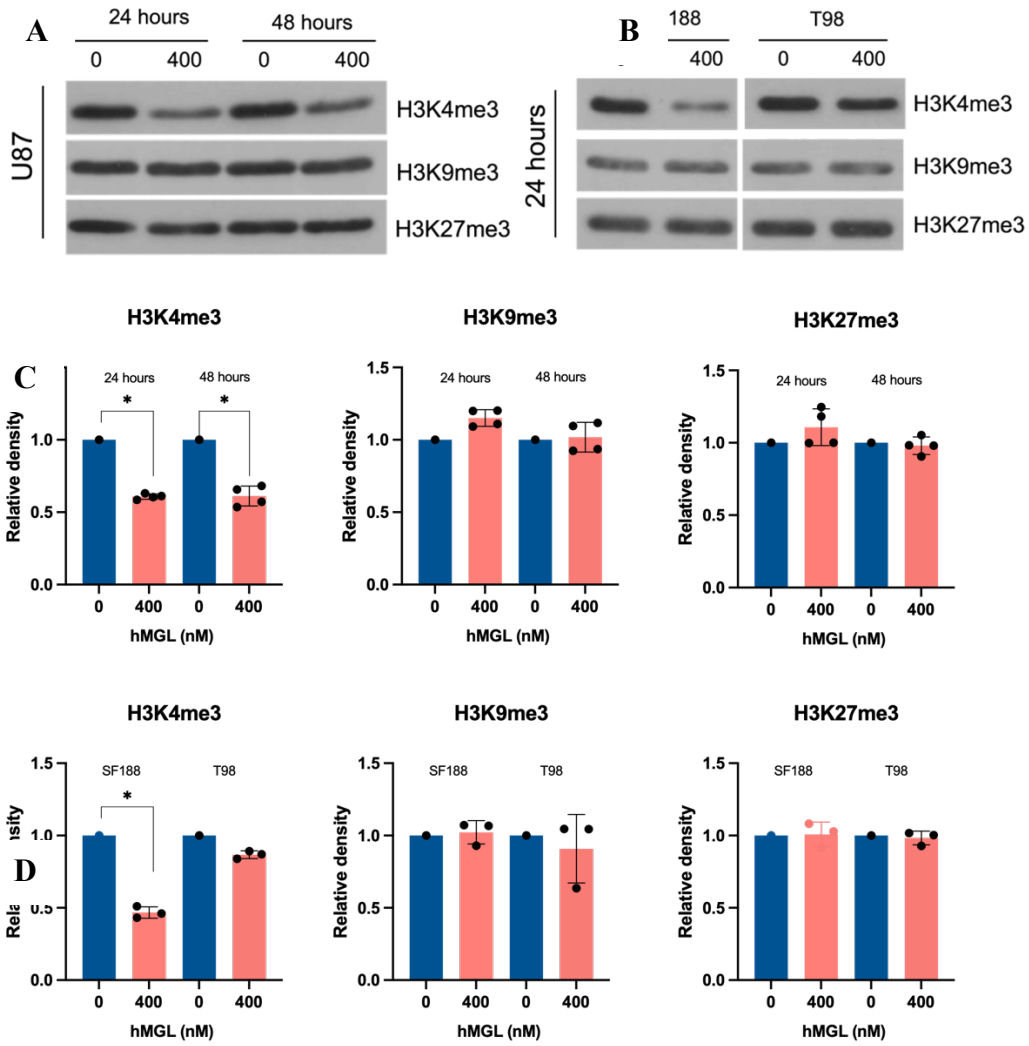

Figure 4.2 hMGL treatment induced demethylation of H3K4me3. H3K4me3, H3K9me3, and H3K27me3 in U87 cells was examined by western blotting. **A, C**. hMGL significantly decreased the amount of H3K4me3 while H3K9me3 and H3K27me3 were not significantly altered. **B, D**. The hMGL-induced modification of histone methylation followed a similar pattern in pediatric GBM cell line SF188. In addition, after 24 hours of treatment with 400 nM hMGL, a visible reduction of H3K4me3 was observed in T98G, although this reduction did not reach statistical significance. H3K9me3 and H3K27me3 remained stable after 24 hours of hMGL treatment in all cell lines.

4.2.3 hMGL upregulates key tumor suppressive miRNAs in GBM

Since hMGL treatment is capable of inducing a substantial decrease in DNA methylation in GBM cells (**Figure 4.1**), we next investigated whether this treatment would result in the re-expression/upregulation of key tumor suppressor miRNAs, which are silenced by promoter hypermethylation during gliomagenesis.

We obtained the miRNA expression data of 558 GBM samples and ten normal samples from the Cancer Genome Atlas (TCGA) database and performed differential expression analysis with the "Limma" R package and visualized the results with a volcano plot (**Figure 4.3 A**). MiR-124 and mir-137 were among the most downregulated miRNAs in GBM, consistent with previously reported by Bhaskaran et al.[139] Importantly, an abundance of evidence suggests that both miR-124 and miR-137 inhibit GBM proliferation and induce brain tumor stem cell differentiation. In addition, the promoter regions of both of these microRNAs are hypermethylated in GBM relative to normal brain tissue.[140,141]

In light of these findings, we next investigated whether hMGL treatment increases miR-124a and miR137 expression in GBM cells. U87 cells were treated with 400 nM hMGL for 24 hours, and RT-qPCR was used to quantify miR-124a and miR-137. The expression levels of both miRNAs increased significantly, with mir-124a being upregulated 2.20 times and mir-137 being upregulated 1.25 times (**Figure 4.3 B**).

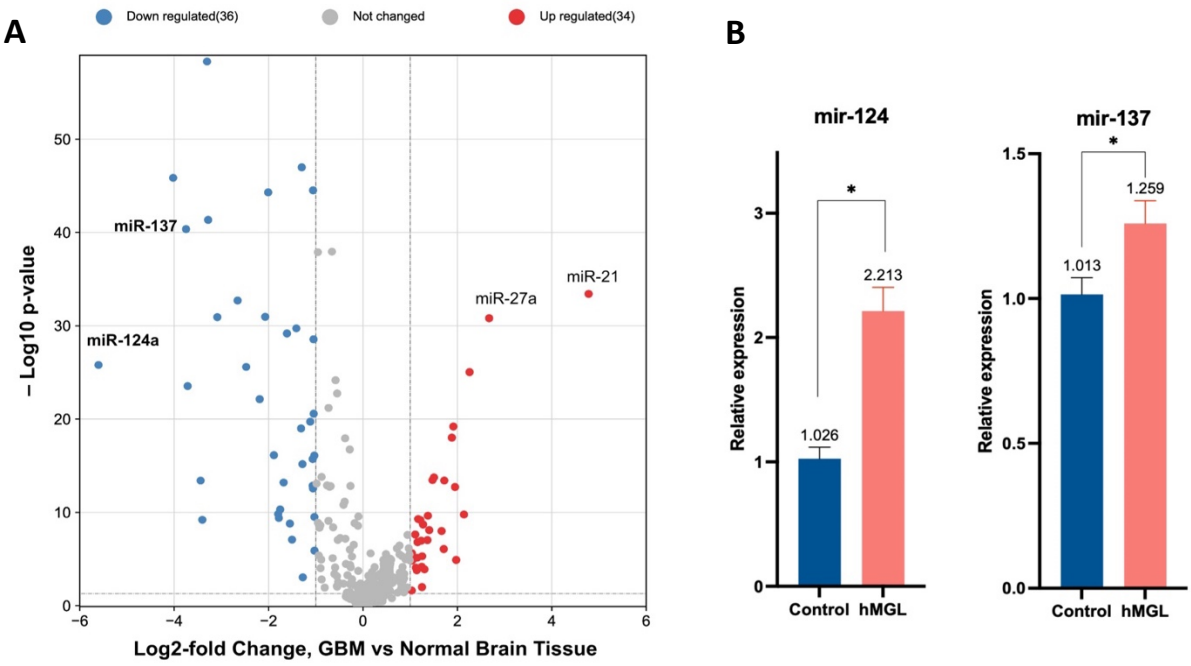

Figure 4.3 hMGL upregulates key tumor suppressive miRNAs in GBM A. Volcano plot show differentially expressed miRNAs between GBM and normal brain tissues. The Cancer Genome Atlas (TCGA) database was queried for microRNA expression information on 558 GBM samples and 10 normal samples, and differential expression analysis was performed using the R package "LIMMA". MiR-124 and mir-137 were among the miRNAs most significantly downregulated in GBM. Volcano plot was plotted by https://www.bioinformatics.com.cn (last accessed on 31 Oct 2022), an online platform for data analysis and visualization. **B**. U87 cells were treated with hMGL for 24 hours, and the expression levels of miR-124a and miR-137 were determined relative to housekeeping gene RNA-U6 using RT-qPCR. The expression levels of both miRNAs increased significantly, with mir-124a upregulated 2.20-fold and mir-137 upregulated 1.25-fold. Data represents mean ± SEM and a Student's t-test was used to compare the treated to untreated controls. Significance is reported as * $p<0.05$.

4.2.4 hMGL inhibits downstream targets of miR-124 and miR-137 in GBM

As described in Section 4.1, miRNAs participate in biological processes by promoting target mRNA degradation and/or inhibiting the proper translation initiation of target genes through specific binding to the 3′ -UTR or coding regions of their target mRNAs. An average miRNA is estimated to have hundreds of evolutionary conserved targets and several times as many non-conserved targets.[142] Enhancer of zeste 2 polycomb repressive complex 2 subunit (EZH2), signal transducer and activator of transcription 3 (STAT3), cyclin dependent kinases 4 (CDK4), and cyclin dependent kinases 6 (CDK6), etc., are examples of well-studied GBM oncogenes targeted by miR-124 and miR-137.[143-146]

Since hMGL increased the levels of miRNAs that target these proteins, we hypothesized that hMGL treatment would inhibit the expression of these downstream targets. To test our hypothesis, we exposed U87 cells to the same dose of hMGL (400 nM) that induced the upregulation of miR-124a and miR-137. At 24 hours, protein levels of EZH2, STAT3, and CDK4/6 were significantly deceased in the hMGL-treated group compared to the control group at both 24 and 48 hr as determined by Western blotting (**Figure 4.4 A, B**).

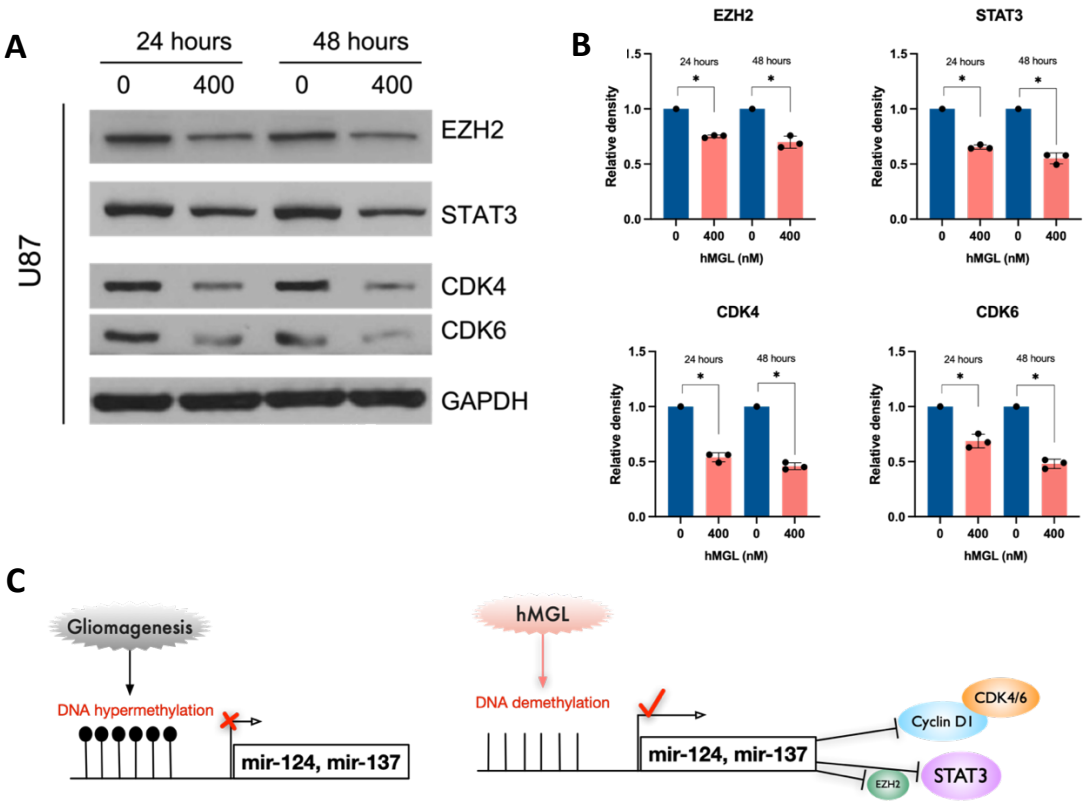

Figure 4.4 hMGL treatment inhibits the expression of miR-124 and miR-137 downstream targets. A, B. U87 cells were exposed to the same concentration of hMGL (400 nM) that upregulated miR-124a and miR-137. Western blotting revealed that after 24 hours, the protein levels of EZH2, STAT3, and CDK4/6 were significantly lower in the hMGL-treated group compared to the control group. Although not statistically significant, it appears that prolonged treatment for up to 48 hours was able to reduce the protein expression levels further. **C.** Schematic illustration of the possible relationship between miRNA-mediated suppression of oncogenes and hMGL-induced DNA hypermethylation release. Promoter hypermethylation silences tumor suppressive miRNAs such as miR-124 and miR-137 during gliomagenesis. The treatment with hMGL reduces DNA methylation, restores the expression of tumor-suppressing miRNAs, and inhibits the expression of oncogenes. Data represents mean ± SEM and a Student's t-test was used to compare the treated to untreated controls. Significance is reported as * $p<0.05$.

4.3 DISCUSSION

These results presented in this chapter provide evidence that the inhibitory effect of hMGL on proliferation of GBM cells involves epigenetic mechanisms. SAM and other metabolic intermediates connect nutrient availability and cellular metabolism to epigenetic regulation and cell signaling pathways. L-Met is the only precursor for SAM; therefore, it is not surprising that depleting L-Met with hMGL will decrease SAM levels, alter the intracellular SAM/SAH ratio, and decrease DNA methylation.

In addition to a decrease in DNA methylation, we also observed a decrease in histone methylation at a particular site, H3K4me3, but not a decrease in histone methylation globally. This is intriguing not only because H3K4me3 is associated with "activate transcribing status", but also because H3K4 is one of the histone methylations sites that serves as a "methyl sink" in eukaryotic cells[132]. Indeed, alongside phosphatidylethanolamine, histone proteins are one of the major consumers of SAM. This allows histones, — in particular H3K4, H3K36, and H3K79, to serve as potential SAM reservoirs. Recently, Ye et al. showed that inhibition of single or combinatorial methylation of H3K4, H3K36, and H3K79 in cells deficient in phospholipid methylation increases SAM levels by 100–200-fold, whereas phospholipid methylation deficiency alone increases SAM levels by 20-fold.[147] Therefore, in response to hMGL treatment, the decrease in H3K4me3 may serve as an important compensatory mechanism to restore SAM hemostasis by releasing SAM to support more essential methylating reactions and supplement nuclear GSH. This may also explain why hMGL was only able to decrease DNA methylation at a higher concentration (**Figure 4.1**).

It should be noted, however, that SAM depletion may not be the only mechanism contributing to the decrease in DNA methylation observed in Section 4.2.1. In fact, accumulation of ROS as a result of GSH depletion can also contribute to global DNA demethylation. As demonstrated in Chapter 3, hMGL treatment depletes GSH by eliminating the substrate supply to the transsulfuration pathway. This disrupts the oxidative equilibrium in GBM cells, resulting in elevated ROS levels. In general, elevated levels of reactive oxygen species are linked to global DNA hypomethylation by altering the activity or expression of DNMTs.[148,149] Moreover, ROS can affect DNA methylation by directly modifying DNA bases; for instance, hydroxyl radicals converts 5mC to 5hmC, which is able to interfere with DNMT1 and result in indirect demethylation of CpG sites.[150,151]

Our data also highlighted the potential functional significance of this hMGL-induced DNA demethylation. We have demonstrated that hMGL treatment upregulated the expression level of two of the most downregulated tumor suppressor miRNAs in GBM, miR-124 and miR-137. MiR-124 and miR-137 functions by promoting the differentiation of neural stem cells and tumor stem cells and inducing cell cycle arrest.[141] Both of these miRNAs are frequently silenced during gliomagenesis by promoter hypermethylation.[136,146,152] One earlier research has shown 5-aza-induced DNA hypomethylation was able to restore expression of this miRNA couple and inhibit GBM growth.[141] In a recent study, Bhaskaran et al. used gene therapy approaches to administer an miRNA cluster comprised of miR-124, miR-137 and miR-128 to GBMs. Their results showed that miRNAs synergistically ablated GBM growth and improved survival in mouse models.[139]

hMGL is more advantageous than small-molecule DNA methylation inhibitors and the gene therapy approach used in the previous research for restoring tumor-suppressing microRNAs in GBMs. First, since hMGL is administered systemically and depletes methionine in the serum, its application is not restricted by the BBB. Also, by depleting SAM, hMGL induces a broad spectrum of DNA demethylation and is able to release multiple miRNAs from their silencing mechanisms, mimicking the synergistic effect of miRNA clusters.

In summary, our preliminary findings indicate that hMGL treatment reduces DNA methylation and trimethylation at H3k4. Alongside this, tumor suppressive miRNAs that are normally silenced by DNA hypermethylation were upregulated in GBM cells. Following with the increase of these tumor-suppressing microRNAs, the protein expression level of downstream oncogenes was also suppressed, providing further evidence of its functional significance **(Figure 4.4 C)**.

Chapter 5: Enhancing hMGL with combination therapies

5.1 INTRODUCTION

In chapters 3 and 4, we investigated the effects of hMGL treatment on GBM cells and possible mechanisms for its actions. Metabolic profiling suggested that disrupted GSH and nucleotide metabolism is associated with the inhibition of GBM survival and proliferation; this is further corroborated by increased DNA damage/replication stress and cell cycle arrest in GBM cells treated with hMGL. As mentioned earlier, a major obstacle in targeting methionine dependency lies in the adaptability and plasticity of cancer metabolism. Indeed, multiple compensatory mechanisms exist for GBM cells to counterbalance these therapeutic effects of hMGL-induced metabolic perturbance. It is therefore necessary and plausible to investigate hMGL as part of a combination therapy.

5.1.1 Targeting the redundant antioxidant pathways in GBM

GBM cell redox homeostasis, for instance, is controlled not only by the GSH system but also by the Trx-dependent system. Previous study has demonstrated that the loss of thioredoxin reductase 1 renders tumors highly susceptible to pharmacologic GSH depletion, suggesting the existence of redundant antioxidant pathways.[153] In addition, Schmidt et al. has demonstrated that either the GSH- or the TrxR1-dependent redox pathway can support cell proliferation independently, using a hepatocyte model. [154] This observation was also corroborated in primary human T cells, where thioredoxin (Trx) can partly substitute for GSH during DNA synthesis.[155]

Therefore, combining hMGL with agents that inhibit the Trx system makes a rational therapeutic strategy. A pharmacologic approach to inhibit the Trx system is to use auranofin (AUR), a potent inhibitor of thioredoxin reductase (Trx) by forming stable, and irreversible, adducts with thiol and selenic groups.[156] In fact, our group has recently shown that combination of AUR and enzyme-mediated depletion of L-cyst(e)ine synergistically kills pancreatic cancer by inducing oxidative stress.[157] However, whether combining hMGL and AUR will be effective in GBM cells, has not yet been investigated.

5.1.2 Targeting replication stress in GBM

GBM cells are also equipped with defense mechanisms to counteract the consequences of excessive ROS and insufficient nucleotide pool. Oxidative stress can cause the majority of DNA damages in human cells including oxidized bases, sugar modifications, DNA or protein crosslinks, and DNA strand breaks.[158]

Together with alteration in the nucleotide pool, DNA damage can halt replication forks and impede DNA replication, causing replication stress. In response to this, cells activate DNA damage repair pathways and block cell cycle progression in order to slow down DNA synthesis and provide time for DNA repair. During replication stress response, ATR is recruited to exposed ssDNA at stalled replication forks by replication protein A (RPA), where it phosphorylates several downstream targets, including CHK1 and H2AX. CHK1 activation promotes fork stabilization and cell cycle checkpoint activation and prevents the replication origin firing until stalled forks are resolved. Activated H2AX, on the other hand, recruits RAD51 at reversed forks in order to protect newly synthesized

DNA tracts and aid in fork restart. [159] Additionally, ATR promotes de novo nucleotide biosynthesis and facilitates the salvaging of preformed nucleosides for dNTP synthesis to compensate for nucleotide deficiency.[160,161] Therefore, the disruption of the ATR-CHK1 axis can exacerbate the replication stress state and permit cell cycle progression despite high levels of unrepaired DNA damage and accumulation of stalled replication forks, resulting in mitotic catastrophe and apoptosis.

Several small molecule inhibitors targeting the replication stress pathway are under development and being evaluated in preclinical and clinicals studies. Available ATR inhibitors (ATRi) include VX-970, AZD6738, BAY1895344, M4344, ART0380, and RP-3500. Among these inhibitors, AZD6738 is an orally active agent that readily crosses the blood-brain barrier and has been demonstrated to inhibit both solid and hematological cell lines with an IC50 of less than 1 nM.

The role of ATR in replication stress suggests ATRis should mechanistically combine well with replication-associated DNA-damaging therapies to potentiate the antitumor activity. Several preclinical studies support this idea where ATRis show activity in combination with IR and chemotherapy agents such as cisplatin, irinotecan, bendamustine, and gemcitabine, as well as PARP inhibitors.[162-167] We hypothesized that hMGL would synergize with AZD6738 in inhibiting GBM cells by inducing DNA damage and replication stress.

Results

5.2.1 hMGL synergizes with AUR in inhibiting GBM cells

To test if targeting TrxR provides a synergistic effect with hMGL in inhibiting GBMs, we treated GBM cells with different concentrations of hMGL concomitantly with AUR in 96-well plates. Cell survival was measured by crystal violet assay after 48 hours of treatment in culture. Treatment with the hMGL and AUR combination is significantly more potent in decreasing cell viability in all cell lines, including U87, U251, LN18 (adult GBMs) and SF188 (pediatric GBM). (**Figure 5.1 A**)

Synergy of drug combinations was further assessed with the widely utilized Bliss independence model. Bliss independence model applies to the probability of cell death and describes how combinations of therapies kill a larger fraction of cancer cells. Consider the use of two drugs A and B in a combination strategy. If the individual inhibitory effects of drug A and B on cell/tumor growth (expressed as fraction affected relative to control) are P_A and P_B, respectively, then the expected inhibitory effect of the combination ($P_{combination}$) can be calculated using the complete additivity of probability theory.

$$P_{combination} = P_A + P_B - P_A \times P_B$$

The observed combined inhibitory effect (derived from the actual drug combination experiment) is then compared with $P_{combination}$. If the observed combined inhibitory effect is greater than $P_{combination}$, it indicates synergy between the two drugs; If the observed combined inhibitory effect is equal to the $P_{combination}$, the two drugs are additive; and finally,

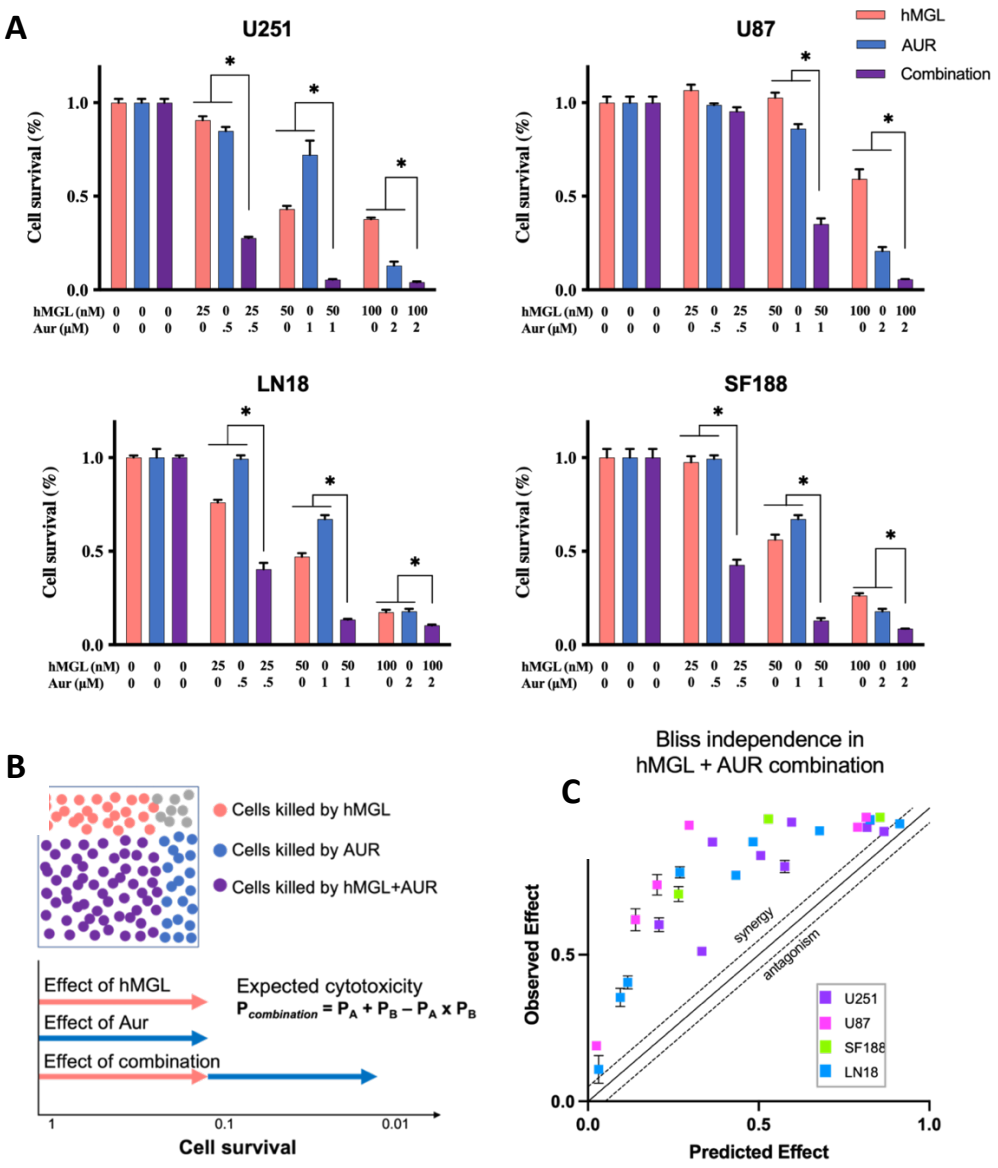

Figure 5.1 hMGL is synergistic with AUR, a TrxR inhibitor. **A**. GBM cells were treated with different concentrations of hMGL concomitantly with AUR. Cell survival was measured by crystal violet assay after 48 hours. Treatment with the hMGL and AUR combination is significantly more potent in decreasing cell viability in all cell lines, including U87, U251, LN18 (adult GBMs) and SF188 (pediatric GBM). **B**. The Bliss independence model was used to evaluate the synergy of drug combinations, and an isobologram was used to visualize the results. The majority of experimental data points fall in the upper left quadrant of the isobologram, indicating synergy between hMGL and AUR across cell lines.

if observed combined inhibitory effect is less than the $P_{combination}$, it indicates that the two drugs are antagonistic with each other (**Figure 5.1 B**).

The extent of synergy attained by two drugs in different cell lines was then visualized using an isobologram. The observed combined inhibitory effect was plotted on the Y-axis, while the expected inhibitory effect was plotted on the X-axis. Most of the experimental data points fell in the upper left portion of the isobologram, indicating synergy between hMGL and AUR across the cell lines (**Figure 5.1 C**).

5.2.2 hMGL synergizes with ATR inhibitor, AZD6738

We next assessed the combination of hMGL with the ATR inhibitor, AZD6738. The rationale is that by disrupting GSH and nucleotide metabolism, hMGL treatment causes DNA damage and replication stress in GBM cells, which will require the activation of ATR-CHK1 axis to halt cell cycle progression and provide sufficient time for DNA repair resolve stalled replication fork.

Using the colony formation assay, the effects of this combination on U87, U251, and LN18 cells were determined. For this purpose, AZD6738 at concentrations of 0.25 μM, 0.5 μM, and 1 μM were used alone or in combination with hMGL at concentrations of 5 nM, 7.5 nM, and 10 nM. A concentration-response matrix was utilized to demonstrate the ability of GBM cells to form colonies under various treatment conditions. By increasing the AZD6738 concentration, the number of colonies was reduced significantly compared to untreated cells. The ability of cells to form colonies was diminished more in cells treated

with both hMGL and AZD6738 than in cells treated with either agent alone. **Figure 5.2 B** displayed a representative image. Bliss independence analysis revealed synergy between hMGL and AZD6738 across all three cell lines, with LN18 exhibiting the most pronounced synergistic effect (**Figure 5.2 C**).

To confirm the mechanism of action underlying the synergy between hMGL and AZD6738, we analyzed the level of g-H2AX, phosphorylated CHK1, and PARP in LN18 cells, the cell line with the strongest synergistic effect. As anticipated, the combination of AZD6738 and hMGL decreased p-CHK1 activation and dramatically increased PARP cleavage. In addition, the level of DNA damage/replication stress marker γ-H2AX in the combination group remained comparable to that of the hMGL-treated group. Taken together, these findings suggest that AZD6738 impeded the cellular response to DNA damage/replication stress by inhibiting the ATR/CHK1 axis and rendered GBM cells more sensitive to hMGL treatment.

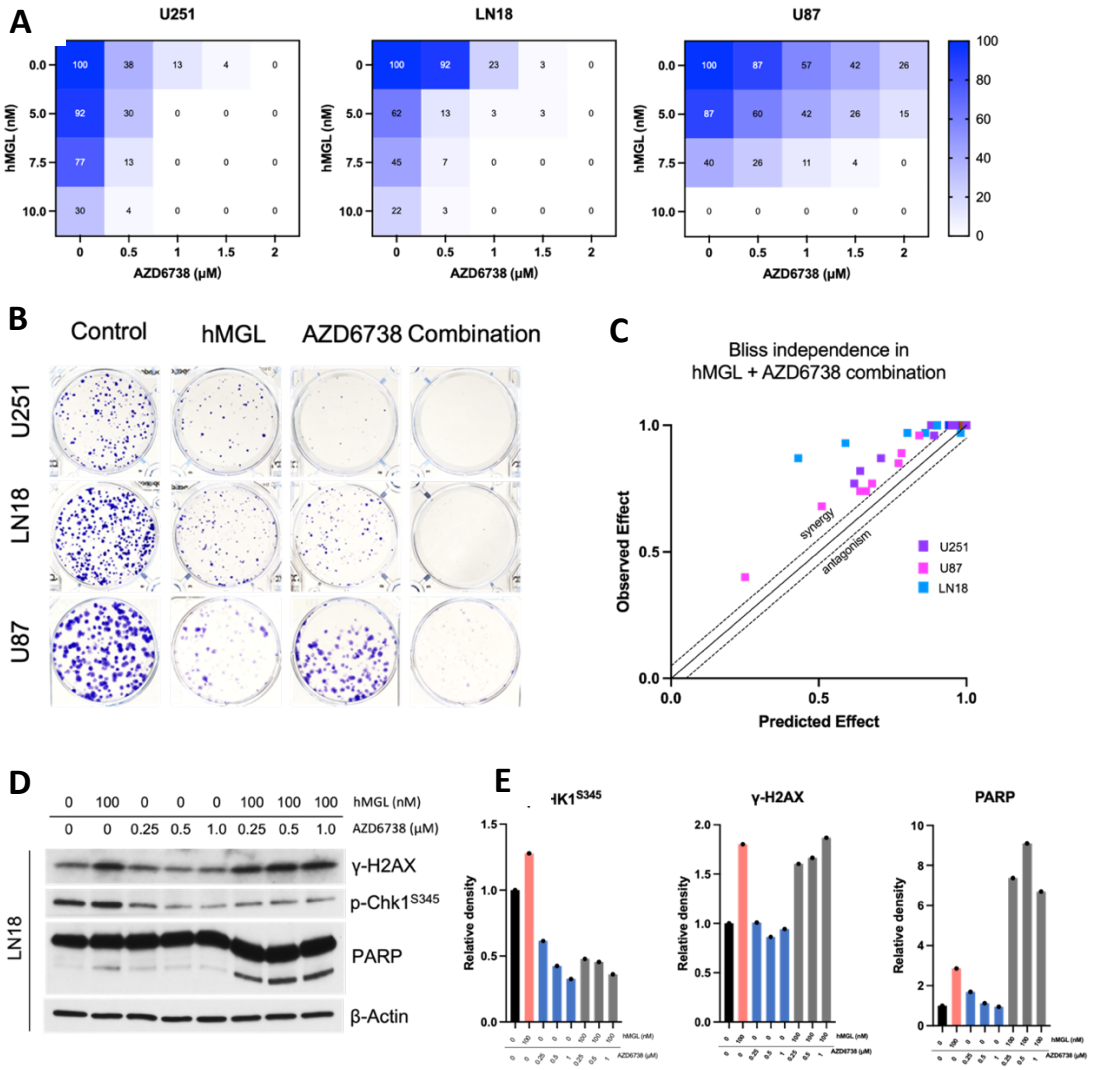

Figure 5.2.2 hMGL synergize with AZD6738, an ATR inhibitor. The effects of the combination on U87, U251, and LN18 cells were determined using the colony formation assay. **A.** Concentration-response matrix illustrates the capacity of GBM cells to form colonies under different treatment conditions. By increasing the concentration of AZD6738, the number of colonies was significantly reduced relative to untreated cells. In cells treated with both hMGL and AZD6738, the ability to form colonies was diminished more than in cells treated with either agent alone. **B.** Representative image of GBM colony formation. **C**. Bliss independence analysis revealed synergy between hMGL and AZD6738 across all three cell lines, with LN18 exhibiting the most pronounced synergistic effect. **D, E.** Western blot show the combination of AZD6738 and hMGL decreased p-CHK1 activation, and dramatically increased PARP cleavage.

5.3 DISCUSSION

Drug combinations have the advantage of counteracting cancer cell compensatory mechanisms by targeting multiple pathways to overcome the toxicity and off-target effects of high doses of single compounds.[78-80] In this chapter, we demonstrated the synergistic effect of combining hMGL with two small molecule agents by targeting two different pathways.

AUR is an FDA-approved gold-based drug that has been used for decades to treat rheumatoid arthritis (RA). Recent drug repurposing research has renewed interest in AUR as a potentially effective cancer treatment. Compared to the creation of a new drug, drug repurposing has numerous advantages. All approved medications have undergone three phases of clinical testing, and their safety and efficacy are guaranteed. In addition, drug repurposing is significantly less expensive than drug development.

In this portion of our experiments, we focused on the pro-oxidative activity of AUR against the thioredoxin reductase system. However, the function of AUR is multifaceted, and we should not overlook the possibility of additional mechanisms underlying its effect. For example, our group has previously reported that on top of enhancing oxidative stress, AUR can also synergize with L-Cys depletion through blocking autophagic flux of cancer cells.[157] Under nutrient deprivation, cells recycle non-essential organelles via autophagy to meet their metabolic requirements. Meanwhile, autophagy also allows cells to recycle defective organelles, which, if left unchecked, would exacerbate oxidative stress. In addition, it has been reported that AUR is able to improve anticancer immune responses at

both cytostatic and cytotoxic concentrations.[168] Thus, future research is required to fully elucidate the mechanism of the hMGL and AUR combination.

Unlike the well-established drug AUR, AZD6738 is a recently developed drug by AstraZeneca to specifically inhibit ATR. Given the importance of ATR in sensing replication stress and activating the S and G2/M checkpoints to facilitate DNA repair, there has been significant interests in studying the response of ATRis in various cancers. Since numerous preclinical studies support the use of ATRi as a DNA-damaging agent sensitizer, it is not surprising that the majority of ongoing clinical trials evaluating ATRis are combination studies (see www.clinicaltrials.gov). The idea is to inhibit ATR in the presence of elevated levels of replication stress and thereby overwhelm the ability of cancer cells to repair damaged DNA.

Our current data demonstrated the effectiveness of this strategy and highlighted the significance of replication stress induction as a mechanism of action for hMGL. hMGL may induce replication stress through a variety of interacting mechanisms, such as increasing oxidative stress, perturbing nucleotide pool, and epigenetic reprogramming. For example, research has shown elevated EZH2 activity and increased H3K27me3 promote degradation of stalled replication forks.[169] Similarly, Set1p and its substrate H3K4me3, also play an important role in genome stability under replication stress.[170] Since hMGL treatment readily changes the histone and DNA methylation patterns, it is necessary to investigate the relationship between replication stress and epigenetic regulation in this

context. How much these mechanisms contribute to the final effect will be the subject of future research.

In summary, we discovered two clinically available small molecule compounds that inhibit GBM growth in a synergistic manner. This provides insight into the mechanism of action of hMGL as well as guidance for future research.

Chapter 6. hMGL inhibits GBM *in vivo*

6.1 Introduction

In this chapter, we utilized orthotopic xenograft models in mice to assess the potential clinical relevance of the findings with hMGL treatment in cell culture models. Since the isolation of U251 cells in 1976, the U251 xenograft model has been used extensively in both intracranial and subcutaneous settings, and it has been published in over 1000 studies[171]. Since the orthotopic injection location provides the murine brain stromal support and an environment most similar to the human tumor site, it is preferred over the heterotopic injection locations.[172] Research has shown that the intracranial orthotopic U251 model accurately recapitulates the histopathology of human GBM after inoculation.[173]

The growth of intracranial xenograft and its response to treatment can be monitored and quantified by bioluminescence imaging (BLI). The U251 cell line, that stably expresses luciferase, was used for orthotopic injections in our studies. At the time of imaging, host mice are injected with luciferin intraperitoneally, which then distributes throughout the mouse body and crosses the blood brain barrier. Luciferase expressed by the xenografted cells uses luciferin as a substrate in a catalytic reaction, leading to the emission of visible light that is detected by the CCD camera of the IVIS imaging system. The intensity of this emitted light correlates to the size of a given xenograft and enables comparisons of xenograft size across different animals, as well as within the same animal over time.

Several studies have demonstrated that bioluminescence- and magnetic resonance-based tumor assessment of drug response in GBM cell line–based xenograft models are highly correlated. For example, Rehemtulla and colleagues reported that tumor burden can be accurately (as confirmed by MRI) assessed using a cost-effective BLI technique in an orthotopic rat xenograft model established by intracranially injection of the 9L-Luc gliosarcoma cell line.[174] Herein, we show that hMGL was able to significantly inhibit the growth in GBM models *in vivo*.

6.2 Results

6.2.1 hMGL inhibits U251-luc GBM orthotopic xenograft *in vivo*

For the experiments, 2 x 10^4 U251-luc cells in 5 μL media were injected into the caudate putamen (CPu, coordination: ML 2 mm, AP 0.5 mm, DV 3.5 MM) of athymic nude mice (n = 11) on a stereotaxic frame. Starting at day-7 post-injection, xenograft growth was monitored with BLI weekly. All mice developed measurable tumor at week 3. On day 26, mice were randomized into "hMGL" and "control" groups and treated with 50 mg/kg hMGL or vehicle every other day via intraperitoneal injection (**Figure 6.1 A**). The dose was determined based on a previous pharmacokinetic study and the efficacy studies performed in models of other cancer types.[75] As shown in **Figure 6.1 C**, hMGL treatment significantly inhibited the growth of U251-luc xenografts compared to the control treatment group. Representative color luminescent images taken at the last imaging session (day 54, treatment for 4 weeks) are shown in **Figure 6.1 B**. As previously reported, hMGL

treated mice did not show any overt signs of toxicity as their body weight stayed constant for the duration of the treatment (**Figure 6.1 D**).

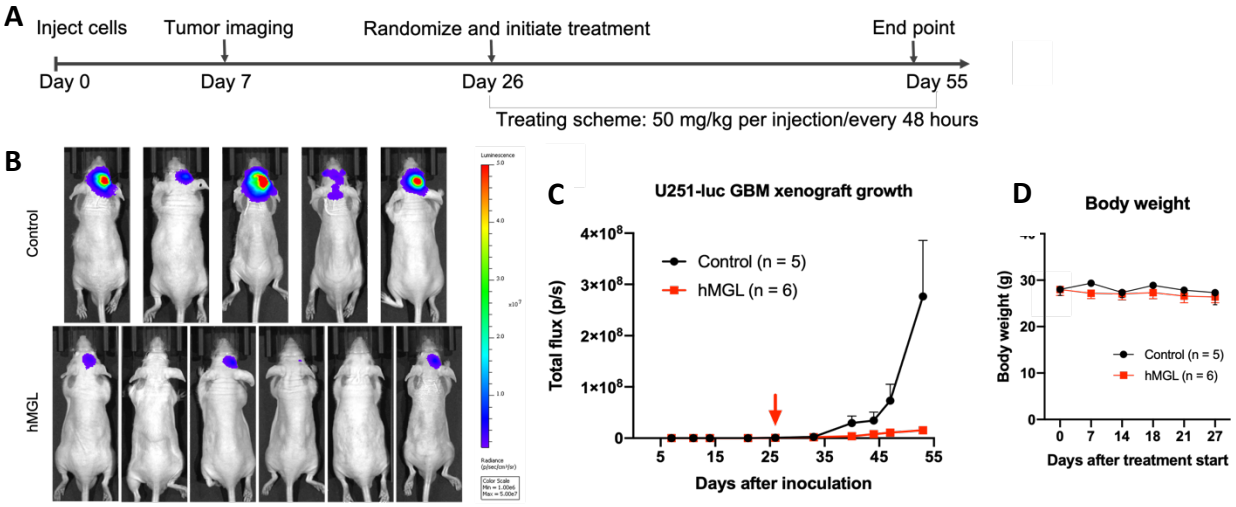

Figure 6.1 hMGL inhibits U251-luc orthotopic GBM xenograft *in vivo*. A. Illustration of the treatment scheme and key time points. **B** Representative bioluminescence images of U251-luc orthotopic GBM xenografts on day 54. **C.** Quantification of the growth of U251-luc orthotopic GBM xenografts as measured by total flux on BLI. Mice treated with hMGL (n =6) experienced significant inhibited growth rate compared with mice treat with vehicle control (n=5). **D.** Average body weight of mice stayed constant for the duration of treatment.

6.2.2 hMGL inhibits GSCs-derived xenografts *in vivo*

In the previous section, we showed that hMGL produced a dramatic inhibition of the growth of the U251-derived orthotopic GBM *in vivo*. As noted in Chapter 1, GBM is composed of heterogeneous tumor cell populations, including glioma stem cells with stem cell properties (GSCs). GSCs are characterized by the expression of neural stem cell markers and the ability to grow as non-adherent spheroids under serum-free conditions in the presence of epidermal growth factor and fibroblast growth factor.[175] GSCs are associated with glioma initiation and drug resistance.[176] Several studies have demonstrated that GSCs are also susceptible to L-Met/SAM deficiency.[177,178] Here, we also examined whether hMGL treatment would inhibit GSC-derived orthotopic xenografts.

To enrich GSCs, U251 cells in monolayer culture were trypsinized into single cells and plated at clonal density in tumor stem media using ultra-low attachment culture dishes. This sphere culture system can limit the secretion of differentiation factors and prevent stimulation of differentiation by adherence.[179,180] Tumor spheroids with tightly connected cells were formed after 10 ~ 14 days. To develop GSC-derived xenografts, spheroids with the diameter between 40 μM and 100 μM were collected and dispersed into single cell suspension after accutase digestion. Again, 2 x 10^4 cells in 5μl were injected into the CPu of athymic nude mice, and beginning on day 7, xenograft development was monitored weekly using BLI. All mice demonstrated measurable tumors seven days after inoculation with cells from spheroids. Mice were subsequently randomized into "hMGL" and "control" groups and administered 50 mg/kg hMGL or vehicle intraperitoneally every other day.

Result show that hMGL also significantly inhibited the growth of orthotopic xenografts produced from GSCs, although to a slightly lesser extent than what was found with monolayer U251-luc cells. Mice treated with hMGL also exhibited significantly prolonged survival compared to vehicle-treated controls.

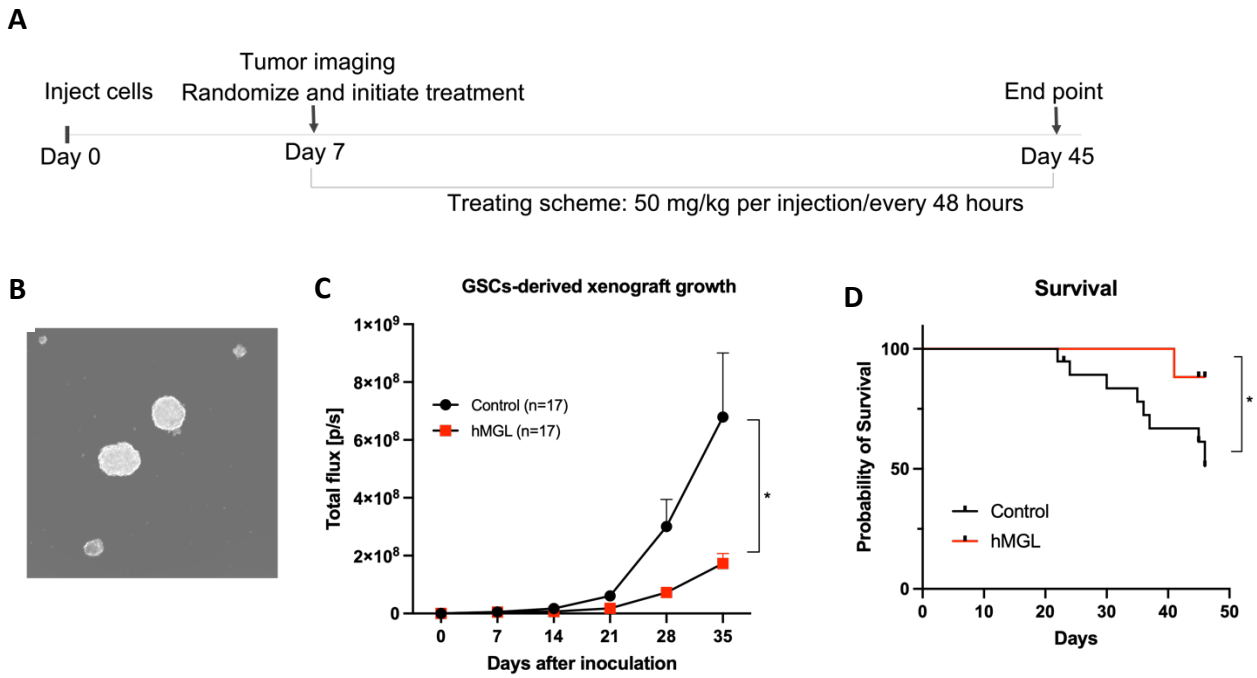

Figure 6.2 hMGL inhibits GSC-derived GBM xenograft *in vivo*. A. Illustration of the treatment scheme and key time points. **B.** Morphology of U251-luc derived tumor spheroids. **C**. Quantification of the growth of GSC-derived xenografts as measured by total flux on BLI. Mice treated with hMGL (n =17) experienced significant inhibited growth rate compared with mice treat with vehicle control (n=17). **D**. Mice treated with hMGL exhibited significantly prolonged survival compared to vehicle-treated controls.

6.2.3 Evaluation of the combination of hMGL and ATRi, AZD6738 in GSCs-derived xenograft model

In Chapter 4, we examined the effects of two combinations on GBM cells: hMGL and the TrxR inhibitor, auranofin, and hMGL and the ATRi, AZD6738. The rationale for hMGL + auranofin is to target redundant ROS scavenging pathways, whereas the rationale for hMGL + AZD6738 is to bypass cancer's DNA damage response mechanisms. Both combinations inhibited GBM growth with significant synergy.

Both auranofin and AZD6738 readily cross the blood-brain barrier and have been evaluated in clinical trials as adjuvant chemotherapies against cancer. [181,182] This encouraged us to investigate whether these drugs could sensitize GBM xenografts to hMGL treatment *in vivo*. Here, we evaluate the hMGL + AZD6738 combination in GSC-derived xenografts, which is relatively less sensitive to U251 parental cell line-derived xenografts (50 mg/kg hMGL inhibited GSC-derived xenograft tumor growth 70% relative to the control group, whereas U251 parental cell line-derived xenografts were inhibited by 95%, see 6.2.1 and 6.2.2). Mice bearing GSC-derived xenografts were randomized into four groups, and were treated with (1) control vehicle, (2) hMGL 50 mg/kg, (3) AZD6738 50 mg/kg, and (4) hMGL 50 mg/kg + AZD6738 50 mg/kg once tumors are measurable by BLI. hMGL were administered via intraperitoneal injection while AZD6738 was given orally by gavage.

Results show that AZD6738 by itself at 50 mg/kg did not result in significant tumor suppression when compared with control. hMGL inhibited xenograft growth by ~80%

when compared to the control group, as calculated by total flux of bioluminescence. This aligns with data presented in 6.2.2. The hMGL and AZD6738 combination also showed great efficacy in inhibiting tumor growth (~85% inhibition). However, the superiority of the combination is not statistically significant when compared with hMGL by itself at the dose tested. Similar to tumor growth data, AZD6738 could not improve animal survival when administered alone. hMGL alone and the hMGL + AZD6738 combination showed comparable effects in improving survival when compared with the control. However, the combination was not superior to hMGL alone in prolonging survival in the GSC-derived xenograft model.

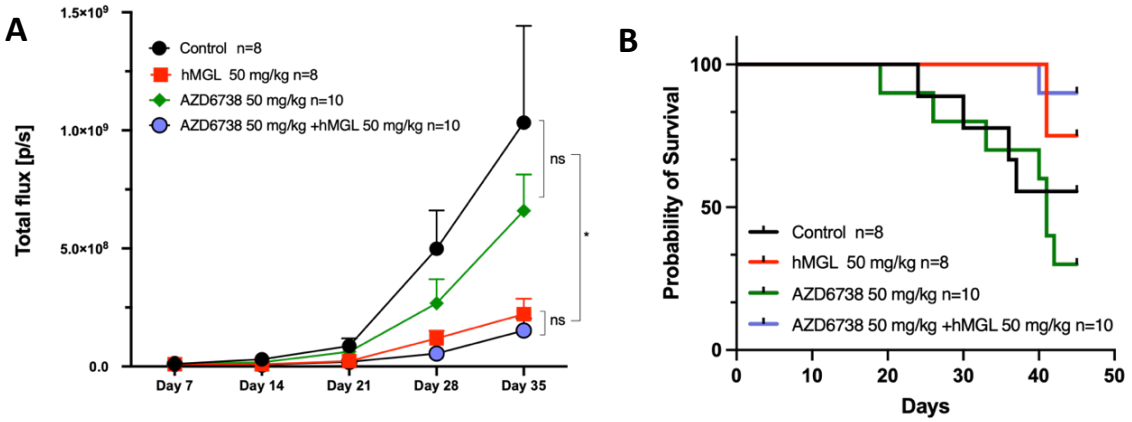

Figure 6.3 Effect of hMGL and AZD6738 combination on GSC-derived GBM xenograft growth and animal survival. A. Mices bearing GSC-derived xenografts were randomized into four groups, and were treated with (1) control vehicle, (2) hMGL 50 mg/kg, (3) AZD6738 50 mg/kg, and (4) hMGL 50 mg/kg + AZD6738 50 mg/kg. Quantification of the growth of GSC-derived xenografts as measured by total flux on BLI. AZD6738 by itself at 50 mg/kg did not result in significant tumor suppression when compared with control. hMGL inhibited xenograft growth by ~80% when compared to the control group. The hMGL and AZD6738 combination also showed great efficacy in inhibiting tumor growth (~85% inhibition). However, the superiority of the combination is non-significant when compared with hMGL by itself. B. AZD6738 could not improve animal survival when administered alone. hMGL alone and the hMGL +AZD6738 combination showed comparable effects in improving survival when compared with the control. However, the combination was not superior to hMGL alone in prolonging survival in the GSC-derived xenograft model.

6.3 DISCUSSION

In this chapter, we evaluated the effect of hMGL treatment on GBM growth *in vivo* using orthotopic xenograft models. We demonstrated that hMGL treatment suppressed xenografts formed with monolayer grown U251 cells, as well as those established with U251 spheroids, which constitute an enriched glioma stem cell-like population.[175] This is in line with previous reports from our group using prostate cancer models and melanoma models.[75] We have observed that hMGL had a more pronounced effect in the U251xenografts compared with the GSC-derived xenografts. This is not surprising given that GSCs have highly efficient clonogenic and tumor initiation capacities and are correlated with the aggressive phenotype of GBMs as well as chemotherapy and radiotherapy resistance.[183-185] Importantly, animals treated with hMGL exhibited no obvious signs of toxicity, as evidenced by their stable body weight throughout the treatment period. Moreover, in the GSC-derived xenograft experiment, hMGL treatment prolonged the survival time of tumor-bearing mice, which is particularly relevant for the treatment of GBM. Collectively, these findings supported the clinical applicability of hMGL as a potential GBM treatment.

Since the combination of hMGL and AZD6738 demonstrated synergy *in vitro*, we evaluated its efficacy in a GSCs-derived xenograft model. We anticipated that AZD6738 would sensitize GSC-derived tumors to hMGL treatment, resulting in an even more potent inhibitory effect. Unfortunately, this *in vivo* tumor model did not replicate the *in vitro* findings. At a dose of 50 mg/kg, hMGL inhibits tumor growth by 80% on its own, which

makes it difficult to observe additional inhibition with the combination. Indeed, the combination of hMGL and AZD6738 inhibited tumor growth by 85%, whereas AZD6738 alone is ineffective against GBM. Further experiments with optimized doses of both hMGL and AZD6738 are required to evaluate this combination's efficacy.

We were unable to evaluate the hMGL and auranofin combination *in vivo* due to time constraints. This does not, however, imply that this combination is unimportant or unpromising. On the contrary, auranofin is an excellent candidate for drug repurposing as a glioblastoma treatment. As described in Chapter 4, auranofin is an FDA-approved drug with a favorable safety profile and good blood-brain barrier permeability.[181] Numerous preclinical studies has demonstrated that auranofin effectively inhibits GBM tumor growth.[186,187] In addition, auranofin just completed a phase Ib/IIa trial and was well tolerated as one of nine repurposed drugs combined with temozolomide for the treatment of recurrent glioblastoma (NCT02770378). A phase II trial is in the planning stages. [188] Consequently, additional experiments should be designed to test the efficacy of the combination of hMGL and auranofin using clinically relevant models.

Chapter 7 Concluding Remarks and Future Directions

7.1 Summary and conclusions

Cancer cells reprogram their metabolic pathways to meet their increased demands for energy production, biomass accumulation, and reducing reactions.[20-22] The metabolic differences between cancer cells and normal tissues can serve as selective therapeutic targets. An emerging aspect of GBM metabolism is the addiction to essential amino acid methionine.[106] The objective of this dissertation was to assess the therapeutic effects and underlying mechanisms of an engineered human methionine-degrading enzyme, hMGL, on glioblastoma.

Our results showed that hMGL treatment selectively inhibited the survival of GBM cells by causing apoptosis. Metabolic profiling and MSEA revealed that aminoacyl tRNA biosynthesis, glutathione metabolism, amino sugar and nucleotide sugar metabolism, and purine metabolism were significantly changed by hMGL treatment.

Following these leads, we discovered that hMGL dramatically decreased GSH levels and induced ROS accumulation in GBM cells. Excessive intracellular ROS harms the cells by damaging DNA, protein, and lipids, and by activating multiple stress signaling pathways. hMGL treatment induced an increase in g-H2AX expression in GBM cells, indicating ongoing DNA damage and replication stress. In accordance with this, cell cycle analysis revealed that hMGL treatment resulted in a S/G2 arrest. The ability of NAC to partially rescue hMGL-treated GBM cells supports the notion that ROS contributed at least partially to the mechanism of action of hMGL. In addition, the uncharged t-RNA pathway

is also involved in the adaptation to hMGL treatment, which is supported by the activation of the eIF2α/ATF4 axis. This is expected because the uncharged t-RNA pathway is a universal means by which cells respond to an insufficiency of amino acids. (Chapter 3)

We also demonstrated that hMGL treatment significantly decreased global DNA methylation and changed histone methylation patterns in GBM cells. GBMs are characterized by aberrant DNA hypermethylation around gene promoters, which typically results in epigenetic silencing of tumor suppressor genes, including tumor suppressing miRNAs.[113-116] In line with this, hMGL treatment led to the upregulation of miR-124 and miR-137, two tumor suppressors that are known to be frequently silenced by promotor hypermethylation in GBMs.[141] Downregulation of oncogene targets of miR-124 and mir-137 further supported the functional importance of the epigenetic reprogramming caused by hMGL treatment. (Chapter 4)

On the basis of the mechanistic implications revealed by our results, we developed two hMGL-based combinations for the treatment of GBM. Both combinations showed synergy in inhibiting GBM growth *in vitro*. Thioredoxin reductase inhibitor auranofin synergizes with hMGL by inhibiting redundant ROS scavenging systems in GBM cells; ATRi AZD6738 synergizes with hMGL by inhibiting DNA repair and cell cycle checkpoints in GBM cells. (Chapter 5)

Finally, the clinical relevance of hMGL was evaluated in human orthotopic GBM xenograft models. We demonstrated that hMGL treatment inhibited xenografts formed

with monolayer U251 cells as well as those established with U251 stem-like cells. We demonstrated that hMGL treatment inhibited xenografts established with both monolayer U251 cells and U251 stem-like cells. In the GSC-derived model, hMGL treatment improved the survival of tumor-bearing animals. (Chapter 6)

In conclusion, targeting methionine metabolism with hMGL shows promise as therapeutic approach for GBM. These findings necessitate further mechanistic analysis and clinical development of hMGL either as single treatment or in combination with other chemotherapeutic agents.

7.2 Future directions

Given the diverse functions of methionine (Figure 1.2), the antitumor effects of MR are unquestionably multifaceted. It is impossible to delineate all the crosstalk and interconnected pathways involved in the inhibitory effect of hMGL within the frame of this work. Future experiments should investigate the mechanism that were not included in the current research.

For example, in nutrient-depleted situations, nutrient recycling and scavenging mechanisms are critical for the survival of cancer cells.[189] The most important of such mechanisms is autophagy, a highly regulated, multi-step process that involves the bulk breakdown of cellular proteins and organelles in order to supply macromolecular precursors and power metabolic pathways. Autophagy has conflicting, context-dependent roles in cancer. On the one hand, autophagy provides an alternative source of intracellular

building blocks and substrates for energy generation, enabling continuous cell survival; on the other hand, autophagic machinery can be recruited to kill cells under certain conditions, resulting in autophagic cell death, a caspase-independent form of programmed cell death (PCD).[190] We have previously observed hMGL-induced autophagy in GBM cells (data not shown), as well as in melanoma and prostate cancer cells.[75] Future research should involve experiments designed to determine the role of autophagy in hMGL-induced methionine depletion. Is it an adaptive process that supports tumor survival, or a consequence of the hMGL therapy that induces inevitable cell death? Should we attempt to stimulate or suppress autophagy? Answers to these questions will shed further light on the mechanisms of hMGL and provide hints for creating hMGL-based combinations.

When designing hMGL-based treatments, we must carefully consider the impact of L-Met depletion on the immune response of cancer. Immune cells such as active T cells require exogenous methionine to synthesize SAM.[191] In fact, cancer cells can "steal" methionine from CD8+ T cells in the tumor microenvironment to inhibit their antitumor activity. Cancer cells are able to outcompete immune cells because they produce large quantities of the methionine transporter SLC43A2.[84] It is therefore possible for immune cells to sustain collateral damage and perish prior to cancer cells being eliminated by hMGL, resulting in immune evasion. We were unable to investigate tumor immune responses to hMGL treatment due to the fact that immuno-deficient mice were utilized in the models employed in this study. Future experiments with genetically engineered models with intact immune systems would help to shed additional light on this aspect.

In addition, although promising from the *in vitro* studies further *in vivo* evaluation of potential synergistic combinations will be necessary. First, there is substantial evidence supporting the safety and efficacy of auranofin in treating GBMs. Additional experiments should be designed to test the efficacy of the combination of hMGL and auranofin using clinically relevant models. Moreover, the hMGL and AZD6738 combination should be re-evaluated using optimized dose for each single agent, but especially optimized doses of hMGL.

References

1 Wen, P. Y. *et al.* Glioblastoma in adults: a Society for Neuro-Oncology (SNO) and European Society of Neuro-Oncology (EANO) consensus review on current management and future directions. *Neuro Oncol* **22**, 1073-1113, doi:10.1093/neuonc/noaa106 (2020).

2 Weller, M. *et al.* EANO guidelines on the diagnosis and treatment of diffuse gliomas of adulthood. *Nat Rev Clin Oncol* **18**, 170-186, doi:10.1038/s41571-020-00447-z (2021).

3 Ostrom, Q. T. *et al.* CBTRUS Statistical Report: Primary Brain and Other Central Nervous System Tumors Diagnosed in the United States in 2015–2019. *Neuro-Oncology* **24**, v1-v95, doi:10.1093/neuonc/noac202 (2022).

4 Stupp, R., Brada, M., Van Den Bent, M., Tonn, J.-C. & Pentheroudakis, G. High-grade glioma: ESMO Clinical Practice Guidelines for diagnosis, treatment and follow-up. *Annals of oncology* **25**, iii93-iii101 (2014).

5 Bagley, S. J. *et al.* Glioblastoma Clinical Trials: Current Landscape and Opportunities for Improvement. *Clin Cancer Res* **28**, 594-602, doi:10.1158/1078-0432.Ccr-21-2750 (2022).

6 Reardon, D. A. *et al.* Effect of Nivolumab vs Bevacizumab in Patients With Recurrent Glioblastoma: The CheckMate 143 Phase 3 Randomized Clinical Trial. *JAMA Oncol* **6**, 1003-1010, doi:10.1001/jamaoncol.2020.1024 (2020).

7 Cloughesy, T. F. *et al.* Effect of Vocimagene Amiretrorepvec in Combination With Flucytosine vs Standard of Care on Survival Following Tumor Resection in Patients With Recurrent High-Grade Glioma: A Randomized Clinical Trial. *JAMA Oncol* **6**, 1939-1946, doi:10.1001/jamaoncol.2020.3161 (2020).

8 Weller, M. *et al.* Rindopepimut with temozolomide for patients with newly diagnosed, EGFRvIII-expressing glioblastoma (ACT IV): a randomised, double-blind, international phase 3 trial. *Lancet Oncol* **18**, 1373-1385, doi:10.1016/s1470-2045(17)30517-x (2017).

9 Narita, Y. *et al.* A randomized, double-blind, phase III trial of personalized peptide vaccination for recurrent glioblastoma. *Neuro Oncol* **21**, 348-359, doi:10.1093/neuonc/noy200 (2019).

10 Lassman, A. B. *et al.* Depatuxizumab-mafodotin in EGFR-amplified newly diagnosed glioblastoma: a phase III randomized clinical trial. *Neuro Oncol*, doi:10.1093/neuonc/noac173 (2022).

11 Roth, P. *et al.* EORTC 1709/CCTG CE.8: A phase III trial of marizomib in combination with temozolomide-based radiochemotherapy versus temozolomide-based radiochemotherapy alone in patients with newly diagnosed glioblastoma. *Journal of Clinical Oncology* **39**, 2004-2004, doi:10.1200/JCO.2021.39.15_suppl.2004 (2021).

12 Tan, A. C. *et al.* Management of glioblastoma: State of the art and future directions. *CA Cancer J Clin* **70**, 299-312, doi:10.3322/caac.21613 (2020).

13 Fisher, J. P. & Adamson, D. C. Current FDA-Approved Therapies for High-Grade Malignant Gliomas. *Biomedicines* **9**, doi:10.3390/biomedicines9030324 (2021).
14 Omuro, A. & DeAngelis, L. M. Glioblastoma and Other Malignant Gliomas: A Clinical Review. *JAMA* **310**, 1842-1850, doi:10.1001/jama.2013.280319 (2013).
15 Tan, A. C. *et al.* Management of glioblastoma: State of the art and future directions. *CA: A Cancer Journal for Clinicians* **70**, 299-312, doi:https://doi.org/10.3322/caac.21613 (2020).
16 Weller, M. *et al.* EANO guideline for the diagnosis and treatment of anaplastic gliomas and glioblastoma. *Lancet Oncol* **15**, e395-403, doi:10.1016/S1470-2045(14)70011-7 (2014).
17 Weller, M. & Le Rhun, E. How did lomustine become standard of care in recurrent glioblastoma? *Cancer Treat Rev* **87**, 102029, doi:10.1016/j.ctrv.2020.102029 (2020).
18 Gatto, L. *et al.* Pharmacotherapeutic Treatment of Glioblastoma: Where Are We to Date? *Drugs* **82**, 491-510, doi:10.1007/s40265-022-01702-6 (2022).
19 Stine, Z. E., Schug, Z. T., Salvino, J. M. & Dang, C. V. Targeting cancer metabolism in the era of precision oncology. *Nat Rev Drug Discov* **21**, 141-162, doi:10.1038/s41573-021-00339-6 (2022).
20 Hanahan, D. & Weinberg, Robert A. Hallmarks of Cancer: The Next Generation. *Cell* **144**, 646-674, doi:https://doi.org/10.1016/j.cell.2011.02.013 (2011).
21 Hanahan, D. Hallmarks of Cancer: New Dimensions. *Cancer Discov* **12**, 31-46, doi:10.1158/2159-8290.Cd-21-1059 (2022).
22 Pavlova, N. N. & Thompson, C. B. The Emerging Hallmarks of Cancer Metabolism. *Cell Metab* **23**, 27-47, doi:10.1016/j.cmet.2015.12.006 (2016).
23 Pavlova, Natalya N. & Thompson, Craig B. The Emerging Hallmarks of Cancer Metabolism. *Cell Metab* **23**, 27-47, doi:https://doi.org/10.1016/j.cmet.2015.12.006 (2016).
24 Pavlova, N. N., Zhu, J. & Thompson, C. B. The hallmarks of cancer metabolism: Still emerging. *Cell Metab* **34**, 355-377, doi:10.1016/j.cmet.2022.01.007 (2022).
25 Panosyan, E. H., Lin, H. J., Koster, J. & Lasky, J. L. In search of druggable targets for GBM amino acid metabolism. *Bmc Cancer* **17**, 162, doi:10.1186/s12885-017-3148-1 (2017).
26 Rosenzweig, A., Blenis, J. & Gomes, A. P. Beyond the Warburg Effect: How Do Cancer Cells Regulate One-Carbon Metabolism? *Front Cell Dev Biol* **6**, 90, doi:10.3389/fcell.2018.00090 (2018).
27 Backlund, P. S., Jr., Chang, C. P. & Smith, R. A. Identification of 2-keto-4-methylthiobutyrate as an intermediate compound in methionine synthesis from 5'-methylthioadenosine. *J Biol Chem* **257**, 4196-4202 (1982).
28 Cone, M. C., Marchitto, K., Zehfus, B. & Ferro, A. J. Utilization by Saccharomyces cerevisiae of 5'-methylthioadenosine as a source of both purine and methionine. *J Bacteriol* **151**, 510-515 (1982).

29 Gao, X., Reid, M. A., Kong, M. & Locasale, J. W. Metabolic interactions with cancer epigenetics. *Mol Aspects Med* **54**, 50-57, doi:10.1016/j.mam.2016.09.001 (2017).
30 Ducker, G. S. & Rabinowitz, J. D. One-Carbon Metabolism in Health and Disease. *Cell Metab* **25**, 27-42, doi:10.1016/j.cmet.2016.08.009 (2017).
31 Palanichamy, K. *et al.* Methionine and Kynurenine Activate Oncogenic Kinases in Glioblastoma, and Methionine Deprivation Compromises Proliferation. *Clin Cancer Res* **22**, 3513-3523, doi:10.1158/1078-0432.Ccr-15-2308 (2016).
32 Hoffman, R. M. Development of recombinant methioninase to target the general cancer-specific metabolic defect of methionine dependence: a 40-year odyssey. *Expert opinion on biological therapy* **15**, 21-31 (2015).
33 Cavuoto, P. & Fenech, M. F. A review of methionine dependency and the role of methionine restriction in cancer growth control and life-span extension. *Cancer Treat Rev* **38**, 726-736, doi:10.1016/j.ctrv.2012.01.004 (2012).
34 Kokkinakis, D., Von Wronski, M., Vuong, T., Brent, T. & Schold Jr, S. Regulation of O 6-methylguanine-DNA methyltransferase by methionine in human tumour cells. *British journal of cancer* **75**, 779 (1997).
35 Aki, T. *et al.* Evaluation of brain tumors using dynamic 11C-methionine-PET. *J Neurooncol* **109**, 115-122, doi:10.1007/s11060-012-0873-9 (2012).
36 TÓTh, G. *et al.* DETECTION OF PROSTATE CANCER WITH 11C-METHIONINE POSITRON EMISSION TOMOGRAPHY. *Journal of Urology* **173**, 66-69, doi:10.1097/01.ju.0000148326.71981.44 (2005).
37 Kaste, S. C. *et al.* Comparison of (11)C-Methionine and (18)F-FDG PET/CT for Staging and Follow-up of Pediatric Lymphoma. *J Nucl Med* **58**, 419-424, doi:10.2967/jnumed.116.178640 (2017).
38 Nawashiro, H. *et al.* High expression of L-type amino acid transporter 1 in infiltrating glioma cells. *Brain Tumor Pathology* **22**, 89-91, doi:10.1007/s10014-005-0188-z (2005).
39 Kim, S. *et al.* 11C-methionine PET as a prognostic marker in patients with glioma: comparison with 18F-FDG PET. *Eur J Nucl Med Mol Imaging* **32**, 52-59, doi:10.1007/s00259-004-1598-6 (2005).
40 Hatakeyama, T. *et al.* 11C-methionine (MET) and 18F-fluorothymidine (FLT) PET in patients with newly diagnosed glioma. *Eur J Nucl Med Mol Imaging* **35**, 2009-2017, doi:10.1007/s00259-008-0847-5 (2008).
41 Kameyama, M. *et al.* The accumulation of 11C-methionine in cerebral glioma patients studied with PET. *Acta Neurochir (Wien)* **104**, 8-12 (1990).
42 Kaschten, B. *et al.* Preoperative evaluation of 54 gliomas by PET with fluorine-18-fluorodeoxyglucose and/or carbon-11-methionine. *J Nucl Med* **39**, 778-785 (1998).
43 Ogawa, T. *et al.* Clinical positron emission tomography for brain tumors: comparison of fludeoxyglucose F 18 and L-methyl-11C-methionine. *AJNR Am J Neuroradiol* **17**, 345-353 (1996).
44 Borbély, K., Nyáry, I., Tóth, M., Ericson, K. & Gulyás, B. Optimization of semi-quantification in metabolic PET studies with 18F-fluorodeoxyglucose and 11C-

methionine in the determination of malignancy of gliomas. *J Neurol Sci* **246**, 85-94, doi:10.1016/j.jns.2006.02.015 (2006).
45 Ogawa, T. *et al.* Carbon-11-methionine PET evaluation of intracerebral hematoma: distinguishing neoplastic from non-neoplastic hematoma. *J Nucl Med* **36**, 2175-2179 (1995).
46 Wang, Z. *et al.* Methionine is a metabolic dependency of tumor-initiating cells. *Nat Med* **25**, 825-837, doi:10.1038/s41591-019-0423-5 (2019).
47 Strekalova, E. *et al.* S-adenosylmethionine biosynthesis is a targetable metabolic vulnerability of cancer stem cells. *Breast Cancer Res Treat* **175**, 39-50, doi:10.1007/s10549-019-05146-7 (2019).
48 Eckert, M. A. *et al.* Proteomics reveals NNMT as a master metabolic regulator of cancer-associated fibroblasts. *Nature* **569**, 723-728, doi:10.1038/s41586-019-1173-8 (2019).
49 Zhang, H., Chen, Z. H. & Savarese, T. M. Codeletion of the genes for p16INK4, methylthioadenosine phosphorylase, interferon-alpha1, interferon-beta1, and other 9p21 markers in human malignant cell lines. *Cancer Genet Cytogenet* **86**, 22-28, doi:10.1016/0165-4608(95)00157-3 (1996).
50 Durie, B. G., Salmon, S. E. & Russell, D. H. Polyamines as markers of response and disease activity in cancer chemotherapy. *Cancer Res* **37**, 214-221 (1977).
51 Gerhauser, C. *et al.* Rotenoids mediate potent cancer chemopreventive activity through transcriptional regulation of ornithine decarboxylase. *Nat Med* **1**, 260-266, doi:10.1038/nm0395-260 (1995).
52 Gupta, S., Ahmad, N., Mohan, R. R., Husain, M. M. & Mukhtar, H. Prostate cancer chemoprevention by green tea: in vitro and in vivo inhibition of testosterone-mediated induction of ornithine decarboxylase. *Cancer Res* **59**, 2115-2120 (1999).
53 Mohan, R. R. *et al.* Overexpression of ornithine decarboxylase in prostate cancer and prostatic fluid in humans. *Clin Cancer Res* **5**, 143-147 (1999).
54 Razin, A. & Cedar, H. DNA methylation and gene expression. *Microbiol Rev* **55**, 451-458 (1991).
55 Jambhekar, A., Dhall, A. & Shi, Y. Roles and regulation of histone methylation in animal development. *Nat Rev Mol Cell Biol* **20**, 625-641, doi:10.1038/s41580-019-0151-1 (2019).
56 Mazor, K. M. *et al.* Effects of single amino acid deficiency on mRNA translation are markedly different for methionine versus leucine. *Sci Rep* **8**, 8076, doi:10.1038/s41598-018-26254-2 (2018).
57 Zou, K., Ouyang, Q., Li, H. & Zheng, J. A global characterization of the translational and transcriptional programs induced by methionine restriction through ribosome profiling and RNA-seq. *BMC Genomics* **18**, 189, doi:10.1186/s12864-017-3483-2 (2017).
58 Aregger, M. & Cowling, V. H. Regulation of mRNA capping in the cell cycle. *RNA Biol* **14**, 11-14, doi:10.1080/15476286.2016.1251540 (2017).

59 Varshney, D. *et al.* mRNA Cap Methyltransferase, RNMT-RAM, Promotes RNA Pol II-Dependent Transcription. *Cell Rep* **23**, 1530-1542, doi:10.1016/j.celrep.2018.04.004 (2018).
60 Laxman, S. *et al.* Sulfur amino acids regulate translational capacity and metabolic homeostasis through modulation of tRNA thiolation. *Cell* **154**, 416-429, doi:10.1016/j.cell.2013.06.043 (2013).
61 Sun, T., Wu, R. & Ming, L. The role of m6A RNA methylation in cancer. *Biomed Pharmacother* **112**, 108613, doi:10.1016/j.biopha.2019.108613 (2019).
62 Goseki, N. *et al.* Synergistic effect of methionine-depleting total parenteral nutrition with 5-fluorouracil on human gastric cancer: a randomized, prospective clinical trial. *Jpn J Cancer Res* **86**, 484-489, doi:10.1111/j.1349-7006.1995.tb03082.x (1995).
63 Thivat, E. *et al.* Phase II trial of the association of a methionine-free diet with cystemustine therapy in melanoma and glioma. *Anticancer research* **29**, 5235-5240 (2009).
64 Tan, Y. *et al.* Anticancer efficacy of methioninase in vivo. *Anticancer research* **16**, 3931-3936 (1996).
65 Tan, Y. *et al.* Overexpression and Large-Scale Production of Recombinantl-Methionine-α-deamino-γ-mercaptomethane-lyase for Novel Anticancer Therapy. *Protein expression and purification* **9**, 233-245 (1997).
66 Lishko, V. K., Lishko, O. V. & Hoffman, R. M. Depletion of serum methionine by methioninase in mice. *Anticancer research* **13**, 1465-1468 (1993).
67 Hu, J. & Cheung, N. K. V. Methionine depletion with recombinant methioninase: in vitro and in vivo efficacy against neuroblastoma and its synergism with chemotherapeutic drugs. *International journal of cancer* **124**, 1700-1706 (2009).
68 Kreis, W. & Hession, C. Isolation and purification of L-methionine-alpha-deamino-gamma-mercaptomethane-lyase (L-methioninase) from Clostridium sporogenes. *Cancer Res* **33**, 1862-1865 (1973).
69 Tan, Y. *et al.* Overexpression and large-scale production of recombinant L-methionine-alpha-deamino-gamma-mercaptomethane-lyase for novel anticancer therapy. *Protein Expr Purif* **9**, 233-245, doi:10.1006/prep.1996.0700 (1997).
70 Yang, Z. *et al.* Pharmacokinetics, methionine depletion, and antigenicity of recombinant methioninase in primates. *Clinical Cancer Research* **10**, 2131-2138 (2004).
71 Yang, Z. *et al.* PEGylation confers greatly extended half-life and attenuated immunogenicity to recombinant methioninase in primates. *Cancer research* **64**, 6673-6678 (2004).
72 Yang, Z. *et al.* Circulating half-life of PEGylated recombinant methioninase holoenzyme is highly dose dependent on cofactor pyridoxal-5′-phosphate. *Cancer research* **64**, 5775-5778 (2004).
73 Gay, F. *et al.* Methionine tumor starvation by erythrocyte-encapsulated methionine gamma-lyase activity controlled with per os vitamin B6. *Cancer Med* **6**, 1437-1452, doi:10.1002/cam4.1086 (2017).

74 Stone, E. *et al.* De Novo Engineering of a Human Cystathionine-γ-Lyase for Systemic l-Methionine Depletion Cancer Therapy. *Acs Chem Biol* **7**, 1822-1829, doi:10.1021/cb300335j (2012).
75 Lu, W. C. *et al.* Enzyme-mediated depletion of serum l-Met abrogates prostate cancer growth via multiple mechanisms without evidence of systemic toxicity. *Proc Natl Acad Sci U S A* **117**, 13000-13011, doi:10.1073/pnas.1917362117 (2020).
76 Bayat Mokhtari, R. *et al.* Combination therapy in combating cancer. *Oncotarget* **8**, 38022-38043, doi:10.18632/oncotarget.16723 (2017).
77 Frei, E., 3rd *et al.* The effectiveness of combinations of antileukemic agents in inducing and maintaining remission in children with acute leukemia. *Blood* **26**, 642-656 (1965).
78 Sharom, J. R., Bellows, D. S. & Tyers, M. From large networks to small molecules. *Curr Opin Chem Biol* **8**, 81-90, doi:10.1016/j.cbpa.2003.12.007 (2004).
79 Kaelin, W. G. The Concept of Synthetic Lethality in the Context of Anticancer Therapy. *Nature Reviews Cancer* **5**, 689-698, doi:10.1038/nrc1691 (2005).
80 Fang, B. Development of synthetic lethality anticancer therapeutics. *J Med Chem* **57**, 7859-7873, doi:10.1021/jm500415t (2014).
81 Kokkinakis, D. M. *et al.* Synergy between Methionine Stress and Chemotherapy in the Treatment of Brain Tumor Xenografts in Athymic Mice1. *Cancer Research* **61**, 4017-4023 (2001).
82 Kimmelman, A. C. & White, E. Autophagy and Tumor Metabolism. *Cell Metab* **25**, 1037-1043, doi:10.1016/j.cmet.2017.04.004 (2017).
83 Albers, E. Metabolic characteristics and importance of the universal methionine salvage pathway recycling methionine from 5'-methylthioadenosine. *IUBMB Life* **61**, 1132-1142, doi:10.1002/iub.278 (2009).
84 Bian, Y. *et al.* Cancer SLC43A2 alters T cell methionine metabolism and histone methylation. *Nature* **585**, 277-282, doi:10.1038/s41586-020-2682-1 (2020).
85 Poirson-Bichat, F., Gonfalone, G., Bras-Goncalves, R. A., Dutrillaux, B. & Poupon, M. F. Growth of methionine-dependent human prostate cancer (PC-3) is inhibited by ethionine combined with methionine starvation. *Br J Cancer* **75**, 1605-1612, doi:10.1038/bjc.1997.274 (1997).
86 Skordi, E. *et al.* Analysis of time-related metabolic fluctuations induced by ethionine in the rat. *J Proteome Res* **6**, 4572-4581, doi:10.1021/pr070268q (2007).
87 Hibino, Y., Kawarabayashi, Y., Kohri, H., Ueda, N. & Tsukagoshi, S. [The mechanism of potentiation of the antitumor effect of 5-fluorouracil by methionine-free intravenous amino acid solution (AO-90) in rats]. *Gan To Kagaku Ryoho* **21**, 2021-2028 (1994).
88 Hoshiya, Y., Kubota, T., Inada, T., Kitajima, M. & Hoffman, R. M. Methionine-depletion modulates the efficacy of 5-fluorouracil in human gastric cancer in nude mice. *Anticancer Res* **17**, 4371-4375 (1997).
89 Kokkinakis, D. M. *et al.* Synergy between methionine stress and chemotherapy in the treatment of brain tumor xenografts in athymic mice. *Cancer Res* **61**, 4017-4023 (2001).

90 Miousse, I. R. *et al.* Modulation of dietary methionine intake elicits potent, yet distinct, anticancer effects on primary versus metastatic tumors. *Carcinogenesis* **39**, 1117-1126, doi:10.1093/carcin/bgy085 (2018).
91 Gao, X. *et al.* Dietary methionine influences therapy in mouse cancer models and alters human metabolism. *Nature* **572**, 397-401, doi:10.1038/s41586-019-1437-3 (2019).
92 Orillion, A. *et al.* Dietary Protein Restriction Reprograms Tumor-Associated Macrophages and Enhances Immunotherapy. *Clin Cancer Res* **24**, 6383-6395, doi:10.1158/1078-0432.CCR-18-0980 (2018).
93 Durando, X. *et al.* Dietary methionine restriction with FOLFOX regimen as first line therapy of metastatic colorectal cancer: a feasibility study. *Oncology* **78**, 205-209, doi:10.1159/000313700 (2010).
94 Durando, X. *et al.* Optimal methionine-free diet duration for nitrourea treatment: a Phase I clinical trial. *Nutr Cancer* **60**, 23-30, doi:10.1080/01635580701525877 (2008).
95 Thivat, E. *et al.* Phase II trial of the association of a methionine-free diet with cystemustine therapy in melanoma and glioma. *Anticancer Res* **29**, 5235-5240 (2009).
96 Lu, W.-C. *et al.* Enzyme-mediated depletion of serum l-Met abrogates prostate cancer growth via multiple mechanisms without evidence of systemic toxicity. *Proceedings of the National Academy of Sciences* **117**, 13000-13011, doi:doi:10.1073/pnas.1917362117 (2020).
97 Sweeney, S. R. *et al.* Identification of a synergistic combination of dimethylaminoparthenolide and shikonin alters metabolism and inhibits proliferation of pediatric precursor-B cell acute lymphoblastic leukemia. *Mol Carcinog* **59**, 399-411, doi:10.1002/mc.23163 (2020).
98 Patel, A. P. *et al.* Single-cell RNA-seq highlights intratumoral heterogeneity in primary glioblastoma. *Science* **344**, 1396-1401, doi:10.1126/science.1254257 (2014).
99 Verhaak, R. G. *et al.* Integrated genomic analysis identifies clinically relevant subtypes of glioblastoma characterized by abnormalities in PDGFRA, IDH1, EGFR, and NF1. *Cancer Cell* **17**, 98-110, doi:10.1016/j.ccr.2009.12.020 (2010).
100 Neftel, C. *et al.* An Integrative Model of Cellular States, Plasticity, and Genetics for Glioblastoma. *Cell* **178**, 835-849.e821, doi:10.1016/j.cell.2019.06.024 (2019).
101 Pang, Z. *et al.* Using MetaboAnalyst 5.0 for LC–HRMS spectra processing, multi-omics integration and covariate adjustment of global metabolomics data. *Nature Protocols* **17**, 1735-1761, doi:10.1038/s41596-022-00710-w (2022).
102 Pang, Z. *et al.* MetaboAnalyst 5.0: narrowing the gap between raw spectra and functional insights. *Nucleic Acids Research* **49**, W388-W396, doi:10.1093/nar/gkab382 (2021).
103 Ezeriņa, D., Takano, Y., Hanaoka, K., Urano, Y. & Dick, T. P. N-Acetyl Cysteine Functions as a Fast-Acting Antioxidant by Triggering Intracellular H(2)S and

Sulfane Sulfur Production. *Cell Chem Biol* **25**, 447-459.e444, doi:10.1016/j.chembiol.2018.01.011 (2018).
104 Venkatachalam, G., Surana, U. & Clément, M. V. Replication stress-induced endogenous DNA damage drives cellular senescence induced by a sub-lethal oxidative stress. *Nucleic Acids Res* **45**, 10564-10582, doi:10.1093/nar/gkx684 (2017).
105 Zeman, M. K. & Cimprich, K. A. Causes and consequences of replication stress. *Nat Cell Biol* **16**, 2-9, doi:10.1038/ncb2897 (2014).
106 Sowers, M. L. & Sowers, L. C. Glioblastoma and Methionine Addiction. *International Journal of Molecular Sciences* **23**, 7156 (2022).
107 Perillo, B. *et al.* ROS in cancer therapy: the bright side of the moon. *Experimental & Molecular Medicine* **52**, 192-203, doi:10.1038/s12276-020-0384-2 (2020).
108 Jones, P. A. & Baylin, S. B. The Epigenomics of Cancer. *Cell* **128**, 683-692, doi:10.1016/j.cell.2007.01.029 (2007).
109 Kloosterhof, N. K. *et al.* Molecular subtypes of glioma identified by genome-wide methylation profiling. *Genes, Chromosomes and Cancer* **52**, 665-674, doi:https://doi.org/10.1002/gcc.22062 (2013).
110 Jones, P. A. Functions of DNA methylation: islands, start sites, gene bodies and beyond. *Nature Reviews Genetics* **13**, 484-492, doi:10.1038/nrg3230 (2012).
111 Lövkvist, C., Dodd, I. B., Sneppen, K. & Haerter, J. O. DNA methylation in human epigenomes depends on local topology of CpG sites. *Nucleic Acids Research* **44**, 5123-5132, doi:10.1093/nar/gkw124 (2016).
112 Bird, A. DNA methylation patterns and epigenetic memory. *Genes Dev* **16**, 6-21, doi:10.1101/gad.947102 (2002).
113 Berdasco, M. & Esteller, M. Aberrant epigenetic landscape in cancer: how cellular identity goes awry. *Dev Cell* **19**, 698-711, doi:10.1016/j.devcel.2010.10.005 (2010).
114 Esteller, M. Epigenetic gene silencing in cancer: the DNA hypermethylome. *Hum Mol Genet* **16 Spec No 1**, R50-59, doi:10.1093/hmg/ddm018 (2007).
115 de Souza, C. F. *et al.* A Distinct DNA Methylation Shift in a Subset of Glioma CpG Island Methylator Phenotypes during Tumor Recurrence. *Cell Rep* **23**, 637-651, doi:10.1016/j.celrep.2018.03.107 (2018).
116 Liao, P., Ostrom, Q. T., Stetson, L. & Barnholtz-Sloan, J. S. Models of epigenetic age capture patterns of DNA methylation in glioma associated with molecular subtype, survival, and recurrence. *Neuro-Oncology* **20**, 942-953, doi:10.1093/neuonc/noy003 (2018).
117 Esteller, M. *et al.* Inactivation of the DNA-Repair Gene MGMT and the Clinical Response of Gliomas to Alkylating Agents. *New England Journal of Medicine* **343**, 1350-1354, doi:10.1056/nejm200011093431901 (2000).
118 Xipell, E. *et al.* Endoplasmic reticulum stress-inducing drugs sensitize glioma cells to temozolomide through downregulation of MGMT, MPG, and Rad51. *Neuro-Oncology* **18**, 1109-1119, doi:10.1093/neuonc/now022 (2016).
119 Yu, Z. *et al.* Inhibition of NF-κB results in anti-glioma activity and reduces temozolomide-induced chemoresistance by down-regulating MGMT gene

expression. *Cancer Lett* **428**, 77-89, doi:https://doi.org/10.1016/j.canlet.2018.04.033 (2018).
120 Watanabe, T. *et al.* Aberrant hypermethylation of p14ARF and O6-methylguanine-DNA methyltransferase genes in astrocytoma progression. *Brain Pathol* **17**, 5-10, doi:10.1111/j.1750-3639.2006.00030.x (2007).
121 Lee, S. H. *et al.* Growth inhibitory effect on glioma cells of adenovirus-mediated p16/INK4a gene transfer in vitro and in vivo. *Int J Mol Med* **6**, 559-563 (2000).
122 KOLODZIEJ, M. A. *et al.* NDRG2 and NDRG4 Expression Is Altered in Glioblastoma and Influences Survival in Patients with MGMT-methylated Tumors. *Anticancer Res* **36**, 887-897 (2016).
123 Gömöri, É., Pál, J., Mészáros, I., Dóczi, T. & Matolcsy, A. Epigenetic Inactivation of the hMLH1 Gene in Progression of Gliomas. *Diagnostic Molecular Pathology* **16** (2007).
124 Yamashita, A. S. *et al.* Demethylation and epigenetic modification with 5-azacytidine reduces IDH1 mutant glioma growth in combination with temozolomide. *Neuro Oncol* **21**, 189-200, doi:10.1093/neuonc/noy146 (2019).
125 Kelly, A. D. & Issa, J.-P. J. The promise of epigenetic therapy: reprogramming the cancer epigenome. *Current Opinion in Genetics & Development* **42**, 68-77, doi:https://doi.org/10.1016/j.gde.2017.03.015 (2017).
126 Chiappinelli, K. B., Zahnow, C. A., Ahuja, N. & Baylin, S. B. Combining Epigenetic and Immunotherapy to Combat Cancer. *Cancer Research* **76**, 1683-1689, doi:10.1158/0008-5472.CAN-15-2125 (2016).
127 Coral, S. *et al.* Immunomodulatory activity of SGI-110, a 5-aza-2′-deoxycytidine-containing demethylating dinucleotide. *Cancer Immunology, Immunotherapy* **62**, 605-614, doi:10.1007/s00262-012-1365-7 (2013).
128 Jenuwein, T. & Allis, C. D. Translating the Histone Code. *Science* **293**, 1074-1080, doi:doi:10.1126/science.1063127 (2001).
129 Berger, S. L. The complex language of chromatin regulation during transcription. *Nature* **447**, 407-412, doi:10.1038/nature05915 (2007).
130 Dai, Z., Mentch, S. J., Gao, X., Nichenametla, S. N. & Locasale, J. W. Methionine metabolism influences genomic architecture and gene expression through H3K4me3 peak width. *Nat Commun* **9**, 1955, doi:10.1038/s41467-018-04426-y (2018).
131 Rechtsteiner, A. *et al.* The Histone H3K36 Methyltransferase MES-4 Acts Epigenetically to Transmit the Memory of Germline Gene Expression to Progeny. *PLOS Genetics* **6**, e1001091, doi:10.1371/journal.pgen.1001091 (2010).
132 Ye, C. & Tu, B. P. Sink into the Epigenome: Histones as Repositories That Influence Cellular Metabolism. *Trends in Endocrinology & Metabolism* **29**, 626-637, doi:https://doi.org/10.1016/j.tem.2018.06.002 (2018).
133 Calin, G. A. & Croce, C. M. MicroRNA signatures in human cancers. *Nature Reviews Cancer* **6**, 857-866, doi:10.1038/nrc1997 (2006).

134 Lynam-Lennon, N., Maher, S. G. & Reynolds, J. V. The roles of microRNA in cancer and apoptosis. *Biological Reviews* **84**, 55-71, doi:https://doi.org/10.1111/j.1469-185X.2008.00061.x (2009).
135 Chen, B. *et al.* Roles of microRNA on cancer cell metabolism. *Journal of Translational Medicine* **10**, 228, doi:10.1186/1479-5876-10-228 (2012).
136 Furuta, M. *et al.* miR-124 and miR-203 are epigenetically silenced tumor-suppressive microRNAs in hepatocellular carcinoma. *Carcinogenesis* **31**, 766-776, doi:10.1093/carcin/bgp250 (2009).
137 Silber, J. *et al.* miR-124 and miR-137 inhibit proliferation of glioblastoma multiforme cells and induce differentiation of brain tumor stem cells. *BMC Med* **6**, 14, doi:10.1186/1741-7015-6-14 (2008).
138 Lu, C. & Thompson, Craig B. Metabolic Regulation of Epigenetics. *Cell Metab* **16**, 9-17, doi:https://doi.org/10.1016/j.cmet.2012.06.001 (2012).
139 Bhaskaran, V. *et al.* The functional synergism of microRNA clustering provides therapeutically relevant epigenetic interference in glioblastoma. *Nat Commun* **10**, 442, doi:10.1038/s41467-019-08390-z (2019).
140 Bier, A. *et al.* MicroRNA-137 is downregulated in glioblastoma and inhibits the stemness of glioma stem cells by targeting RTVP-1. *Oncotarget* **4**, 665-676, doi:10.18632/oncotarget.928 (2013).
141 Silber, J. *et al.* miR-124 and miR-137 inhibit proliferation of glioblastoma multiforme cells and induce differentiation of brain tumor stem cells. *BMC Medicine* **6**, 14, doi:10.1186/1741-7015-6-14 (2008).
142 Bentwich, I. *et al.* Identification of hundreds of conserved and nonconserved human microRNAs. *Nat Genet* **37**, 766-770, doi:10.1038/ng1590 (2005).
143 Wei, J. *et al.* miR-124 inhibits STAT3 signaling to enhance T cell-mediated immune clearance of glioma. *Cancer Res* **73**, 3913-3926, doi:10.1158/0008-5472.Can-12-4318 (2013).
144 Jovčevska, I. Sequencing the next generation of glioblastomas. *Crit Rev Clin Lab Sci* **55**, 264-282, doi:10.1080/10408363.2018.1462759 (2018).
145 Sun, J., Zheng, G., Gu, Z. & Guo, Z. MiR-137 inhibits proliferation and angiogenesis of human glioblastoma cells by targeting EZH2. *J Neurooncol* **122**, 481-489, doi:10.1007/s11060-015-1753-x (2015).
146 Bhaskaran, V. *et al.* The functional synergism of microRNA clustering provides therapeutically relevant epigenetic interference in glioblastoma. *Nat Commun* **10**, 442, doi:10.1038/s41467-019-08390-z (2019).
147 Ye, C., Sutter, B. M., Wang, Y., Kuang, Z. & Tu, B. P. A Metabolic Function for Phospholipid and Histone Methylation. *Molecular Cell* **66**, 180-193.e188, doi:https://doi.org/10.1016/j.molcel.2017.02.026 (2017).
148 Cyr, A. R. & Domann, F. E. The redox basis of epigenetic modifications: from mechanisms to functional consequences. *Antioxid Redox Signal* **15**, 551-589, doi:10.1089/ars.2010.3492 (2011).

149 Byrne, M. M., Murphy, R. T. & Ryan, A. W. Epigenetic modulation in the treatment of atherosclerotic disease. *Front Genet* **5**, 364, doi:10.3389/fgene.2014.00364 (2014).
150 Branco, M. R., Ficz, G. & Reik, W. Uncovering the role of 5-hydroxymethylcytosine in the epigenome. *Nat Rev Genet* **13**, 7-13, doi:10.1038/nrg3080 (2011).
151 Madugundu, G. S., Cadet, J. & Wagner, J. R. Hydroxyl-radical-induced oxidation of 5-methylcytosine in isolated and cellular DNA. *Nucleic Acids Res* **42**, 7450-7460, doi:10.1093/nar/gku334 (2014).
152 Tian, Z. *et al.* Hypermethylation-mediated inactivation of miR-124 predicts poor prognosis and promotes tumor growth at least partially through targeting EZH2/H3K27me3 in ESCC. *Clin Exp Metastasis* **36**, 381-391, doi:10.1007/s10585-019-09974-1 (2019).
153 Mandal, P. K. *et al.* Loss of Thioredoxin Reductase 1 Renders Tumors Highly Susceptible to Pharmacologic Glutathione Deprivation. *Cancer Research* **70**, 9505-9514, doi:10.1158/0008-5472.CAN-10-1509 (2010).
154 Prigge, J. R. *et al.* Hepatocyte DNA replication in growing liver requires either glutathione or a single allele of txnrd1. *Free Radic Biol Med* **52**, 803-810, doi:10.1016/j.freeradbiomed.2011.11.025 (2012).
155 Levring, T. B. *et al.* Human CD4+ T cells require exogenous cystine for glutathione and DNA synthesis. *Oncotarget* **6**, 21853-21864, doi:10.18632/oncotarget.5213 (2015).
156 Fan, C. *et al.* Enhancement of auranofin-induced lung cancer cell apoptosis by selenocystine, a natural inhibitor of TrxR1 in vitro and in vivo. *Cell Death Dis* **5**, e1191, doi:10.1038/cddis.2014.132 (2014).
157 Kshattry, S. *et al.* Enzyme-mediated depletion of l-cyst(e)ine synergizes with thioredoxin reductase inhibition for suppression of pancreatic tumor growth. *NPJ Precis Oncol* **3**, 16, doi:10.1038/s41698-019-0088-z (2019).
158 Ziech, D., Franco, R., Pappa, A. & Panayiotidis, M. I. Reactive Oxygen Species (ROS)—Induced genetic and epigenetic alterations in human carcinogenesis. *Mutation Research/Fundamental and Molecular Mechanisms of Mutagenesis* **711**, 167-173, doi:https://doi.org/10.1016/j.mrfmmm.2011.02.015 (2011).
159 Ngoi, N. Y. L., Pham, M. M., Tan, D. S. P. & Yap, T. A. Targeting the replication stress response through synthetic lethal strategies in cancer medicine. *Trends Cancer* **7**, 930-957, doi:10.1016/j.trecan.2021.06.002 (2021).
160 D'Angiolella, V. *et al.* Cyclin F-Mediated Degradation of Ribonucleotide Reductase M2 Controls Genome Integrity and DNA Repair. *Cell* **149**, 1023-1034, doi:https://doi.org/10.1016/j.cell.2012.03.043 (2012).
161 Beyaert, M., Starczewska, E., Van Den Neste, E. & Bontemps, F. A crucial role for ATR in the regulation of deoxycytidine kinase activity. *Biochemical Pharmacology* **100**, 40-50, doi:https://doi.org/10.1016/j.bcp.2015.11.022 (2016).
162 Dunne, V. *et al.* Inhibition of ataxia telangiectasia related-3 (ATR) improves therapeutic index in preclinical models of non-small cell lung cancer (NSCLC)

radiotherapy. *Radiother Oncol* **124**, 475-481, doi:10.1016/j.radonc.2017.06.025 (2017).
163 Vendetti, F. P. *et al.* The orally active and bioavailable ATR kinase inhibitor AZD6738 potentiates the anti-tumor effects of cisplatin to resolve ATM-deficient non-small cell lung cancer in vivo. *Oncotarget* **6**, 44289-44305, doi:10.18632/oncotarget.6247 (2015).
164 Jossé, R. *et al.* ATR inhibitors VE-821 and VX-970 sensitize cancer cells to topoisomerase i inhibitors by disabling DNA replication initiation and fork elongation responses. *Cancer Res* **74**, 6968-6979, doi:10.1158/0008-5472.Can-13-3369 (2014).
165 Young, L. A. *et al.* Differential Activity of ATR and WEE1 Inhibitors in a Highly Sensitive Subpopulation of DLBCL Linked to Replication Stress. *Cancer Res* **79**, 3762-3775, doi:10.1158/0008-5472.Can-18-2480 (2019).
166 Wallez, Y. *et al.* The ATR Inhibitor AZD6738 Synergizes with Gemcitabine In Vitro and In Vivo to Induce Pancreatic Ductal Adenocarcinoma Regression. *Mol Cancer Ther* **17**, 1670-1682, doi:10.1158/1535-7163.Mct-18-0010 (2018).
167 Lloyd, R. L. *et al.* Combined PARP and ATR inhibition potentiates genome instability and cell death in ATM-deficient cancer cells. *Oncogene* **39**, 4869-4883, doi:10.1038/s41388-020-1328-y (2020).
168 Freire Boullosa, L. *et al.* Auranofin reveals therapeutic anticancer potential by triggering distinct molecular cell death mechanisms and innate immunity in mutant p53 non-small cell lung cancer. *Redox Biol* **42**, 101949, doi:10.1016/j.redox.2021.101949 (2021).
169 Leung, K. H., Abou El Hassan, M. & Bremner, R. A rapid and efficient method to purify proteins at replication forks under native conditions. *Biotechniques* **55**, 204-206, doi:10.2144/000114089 (2013).
170 Faucher, D. & Wellinger, R. J. Methylated H3K4, a transcription-associated histone modification, is involved in the DNA damage response pathway. *PLoS Genet* **6**, doi:10.1371/journal.pgen.1001082 (2010).
171 Lenting, K., Verhaak, R., Ter Laan, M., Wesseling, P. & Leenders, W. Glioma: experimental models and reality. *Acta Neuropathol* **133**, 263-282, doi:10.1007/s00401-017-1671-4 (2017).
172 Kim, M. P. *et al.* Generation of orthotopic and heterotopic human pancreatic cancer xenografts in immunodeficient mice. *Nature Protocols* **4**, 1670-1680, doi:10.1038/nprot.2009.171 (2009).
173 Radaelli, E. *et al.* Immunohistopathological and neuroimaging characterization of murine orthotopic xenograft models of glioblastoma multiforme recapitulating the most salient features of human disease. *Histol Histopathol* **24**, 879-891, doi:10.14670/hh-24.879 (2009).
174 Rehemtulla, A. *et al.* Rapid and quantitative assessment of cancer treatment response using in vivo bioluminescence imaging. *Neoplasia* **2**, 491-495, doi:10.1038/sj.neo.7900121 (2000).

175 Lathia, J. D., Mack, S. C., Mulkearns-Hubert, E. E., Valentim, C. L. & Rich, J. N. Cancer stem cells in glioblastoma. *Genes Dev* **29**, 1203-1217, doi:10.1101/gad.261982.115 (2015).
176 Suvà, M. L. & Tirosh, I. The Glioma Stem Cell Model in the Era of Single-Cell Genomics. *Cancer Cell* **37**, 630-636, doi:10.1016/j.ccell.2020.04.001 (2020).
177 Guéant, J.-L. *et al.* Genetic, epigenetic and genomic mechanisms of methionine dependency of cancer and tumor-initiating cells: What could we learn from folate and methionine cycles. *Biochimie* **173**, 123-128, doi:https://doi.org/10.1016/j.biochi.2020.03.015 (2020).
178 Jung, J. *et al.* Nicotinamide metabolism regulates glioblastoma stem cell maintenance. *JCI Insight* **2**, doi:10.1172/jci.insight.90019 (2017).
179 Singh, S. K., Clarke, I. D., Hide, T. & Dirks, P. B. Cancer stem cells in nervous system tumors. *Oncogene* **23**, 7267-7273, doi:10.1038/sj.onc.1207946 (2004).
180 Leis, O. *et al.* Sox2 expression in breast tumours and activation in breast cancer stem cells. *Oncogene* **31**, 1354-1365, doi:10.1038/onc.2011.338 (2012).
181 Madeira, J. M., Bajwa, E., Stuart, M. J., Hashioka, S. & Klegeris, A. Gold drug auranofin could reduce neuroinflammation by inhibiting microglia cytotoxic secretions and primed respiratory burst. *J Neuroimmunol* **276**, 71-79, doi:10.1016/j.jneuroim.2014.08.615 (2014).
182 Fròsina, G. *et al.* ATR kinase inhibitors NVP-BEZ235 and AZD6738 effectively penetrate the brain after systemic administration. *Radiat Oncol* **13**, 76, doi:10.1186/s13014-018-1020-3 (2018).
183 Zarkoob, H., Taube, J. H., Singh, S. K., Mani, S. A. & Kohandel, M. Investigating the link between molecular subtypes of glioblastoma, epithelial-mesenchymal transition, and CD133 cell surface protein. *PLoS One* **8**, e64169, doi:10.1371/journal.pone.0064169 (2013).
184 Murat, A. *et al.* Stem cell-related "self-renewal" signature and high epidermal growth factor receptor expression associated with resistance to concomitant chemoradiotherapy in glioblastoma. *J Clin Oncol* **26**, 3015-3024, doi:10.1200/jco.2007.15.7164 (2008).
185 Zhang, X. *et al.* Targeting role of glioma stem cells for glioblastoma multiforme. *Curr Med Chem* **20**, 1974-1984, doi:10.2174/0929867311320150004 (2013).
186 Van Loenhout, J. *et al.* Auranofin and Cold Atmospheric Plasma Synergize to Trigger Distinct Cell Death Mechanisms and Immunogenic Responses in Glioblastoma. *Cells* **10**, 2936 (2021).
187 Kast, R. E. Glioblastoma invasion, cathepsin B, and the potential for both to be inhibited by auranofin, an old anti-rheumatoid arthritis drug. *Cent Eur Neurosurg* **71**, 139-142, doi:10.1055/s-0029-1242756 (2010).
188 Halatsch, M. E. *et al.* A phase Ib/IIa trial of 9 repurposed drugs combined with temozolomide for the treatment of recurrent glioblastoma: CUSP9v3. *Neurooncol Adv* **3**, vdab075, doi:10.1093/noajnl/vdab075 (2021).

189 Florey, O. & Overholtzer, M. Macropinocytosis and autophagy crosstalk in nutrient scavenging. *Philos Trans R Soc Lond B Biol Sci* **374**, 20180154, doi:10.1098/rstb.2018.0154 (2019).
190 Gozuacik, D. & Kimchi, A. Autophagy and cell death. *Curr Top Dev Biol* **78**, 217-245, doi:10.1016/s0070-2153(06)78006-1 (2007).
191 Roy, D. G. *et al.* Methionine Metabolism Shapes T Helper Cell Responses through Regulation of Epigenetic Reprogramming. *Cell Metab* **31**, 250-266.e259, doi:10.1016/j.cmet.2020.01.006 (2020).